SCALED DOWN MODELLING OF A HORIZONTAL WIND TURBINE FOR A FLOATING WIND TURBINE RESEARCH

A Thesis Submitted to
the Graduate School of
İzmir Institute of Technology
in Partial Fulfillment of the Requirements for the Degree of

MASTER OF SCIENCE

in Mechanical Engineering

by
Serkan EROL

July 2020
İZMİR

ACKNOWLEDGMENTS

Firstly, I would like to thank my supervisor Assoc. Prof. Dr. Ünver Özkol for his supports and advices during my studies and researches. I am also grateful that he gave me opportunity by taking part in his project that positively affected my perspective and studies.

I would like to thank to Asist. Prof. Dr. Sercan Acarer and Dr. Timuçin Eriş for their technical support. In addition, I thank IZTECH Mechanical Engineering Fluid Mechanics Lab. members, Civil Engineering Hydromechanics Lab. members and my friends.

I am also thankful to Northel Company for sharing wind turbine technical data with us.

I would like to thank The Scientific and Technological Research Council of Turkey (TUBITAK) for their financial support. This work is supported by TUBITAK under the grant number 217M451.

I would very much like to thank my parents: Ayten Erol, Sebahattin Erol and my brother: A.Sercan Erol, for their endless support throughout my life.

ABSTRACT

SCALED DOWN MODELLING OF A HORIZONTAL WIND TURBINE FOR A FLOATING WIND TURBINE RESEARCH

Floating wind turbines have to operate under the influence of hydrodynamic and aerodynamic forces which are usually coupled in nature. Due to complicated interactions of wave and wind forces on its structure, predicting motion and performance of a floating wind turbine usually depend on many assumptions. In order to understand the dynamics of the system, experimental studies are required to obtain results by taking into account all parameters. This study is a part of a Tübitak project (217M451) that investigates the dynamics of different floating platforms with a wind turbine attached to it under an atmospheric boundary layer wind profile.

In this thesis, a scaling methodology was used to model a wind turbine to use in experimental studies. Reynolds number discrepancy was demonstrated in floating wind turbine modeling. For this reason, the method was created by using Froude number and tip speed ratio similitude, and geometric, kinematic and dynamic similarity was achieved. According to the created methodology, an onshore wind turbine that has 320kW nominal power was scaled down to be used in experimental studies according to the open sea conditions. Along with the model turbine, a thrust force measuring mechanism, hot-wire sensor travers system and a motion detection method by a video have been realized.

A wave maker and a wind nozzle which are the part of the Tübitak project of which the model turbine described in this thesis will be used, therefore; small description of those are also given in the thesis.

ÖZET

YÜZER RÜZGAR TÜRBİNLERİ ARAŞTIRMASI İÇİN BİR YATAY RÜZGAR TÜRBİNİNİN ÖLÇEKLENDİRİLMİŞ MODELLEMESİ

Yüzer rüzgar türbinleri genellikle doğada birleşmiş hidrodinamik ve aerodinamik kuvvetlerin etkisi altında çalışmak zorundadır. Dalga ve rüzgar kuvvetlerinin yapısı üzerindeki karmaşık etkileşimleri nedeniyle, yüzen bir rüzgar türbininin hareket ve performansının tahmin edilmesi genellikle birçok varsayıma bağlıdır. Sistemin dinamiklerini anlamak için tüm parametreler dikkate alınarak sonuçların elde edilmesi için deneysel çalışmaların yapılması gerekmektedir. Bu çalışma, bir atmosferik sınır tabaka rüzgar profili altında kendisine bağlı bir rüzgar türbini ile farklı yüzen platformların dinamiklerini araştıran Tübitak projesinin (217M451) bir parçasıdır.

Bu tezde, bir rüzgar türbinini modellemek ve deneysel çalışmalarda kullanmak için bir ölçekleme metodolojisi kullanılmıştır. Reynolds sayısı tutarsızlığı, yüzer rüzgar türbini modellemesinde gösterilmiştir. Bu nedenle yöntem Froude sayısı ve kanat uç hızı oranı benzerliği kullanılarak oluşturulmuş, geometrik, kinematik ve dinamik benzerlik sağlanmıştır. Oluşturulan metodolojiye göre, 320kW nominal güce sahip bir kara rüzgar türbini açık deniz koşullarına göre deneysel çalışmalarda kullanılmak üzere ölçeklendirilmiştir. Model türbin ile birlikte bir itme kuvveti ölçüm mekanizması, sıcak-tel sensörü için travers sistemi ve bir video ile hareket algılama yöntemi gerçekleştirilmiştir.

Tübitak projesinin bir parçası olan ve bu tezde tarif edilen model türbinin kullanılacağı dalga yapıcı ve rüzgar nozülü, tezde de küçük bir açıklama olarak verilmiştir.

TABLE OF CONTENTS

APPENDICIES

LIST OF FIGURES

Figure **Page**

LIST OF TABLES

LIST OF SYMBOLS

SYMBOLS

a	axial induction factor
a'	tangential induction factor
AoA	angle of attack
C	wave celerity
C_P	power coefficient
C_T	thrust coefficient
Fr	Froude number
g	gravitational acceleration
L	length
P	power
r	blade sectional radius
R	rotor radius
Re	Reynolds number
T	thrust force
TSR	tip speed ratio
U	velocity
z	height
β	pitch angle at the tip
θ	blade twist angle
θ_p	section pitch angle
λ	scaling ratio
λ_{TSR}	sectional tip speed ratio
ν	kinematic viscosity
ϕ	inflow angle
Ω	rotational speed
ω	tangential velocity at wake

INDICES

∞	free stream
d	disk
L	length
m	model
p	prototype
ref	reference
V	velocity

CHAPTER 1

INTRODUCTION

Population of the world is continuously increasing and we are running out of fossil fuels. With the decreasing fossil resources and increasing environmental pollution, societies have started to turn to renewable energy resources. According to International Renewable Energy Agency, there are six types renewable energy resources which are bioenergy, geothermal, hydropower, marine, solar and wind.

Considering wind energy installation capacities, offshore wind turbines has increased over time compared to total installed capacity, see in Figure 1.1. Wind energy power capacity has been tripled in the last decade. Especially the developments in offshore wind turbines have increased the technological and academic studies in this field.

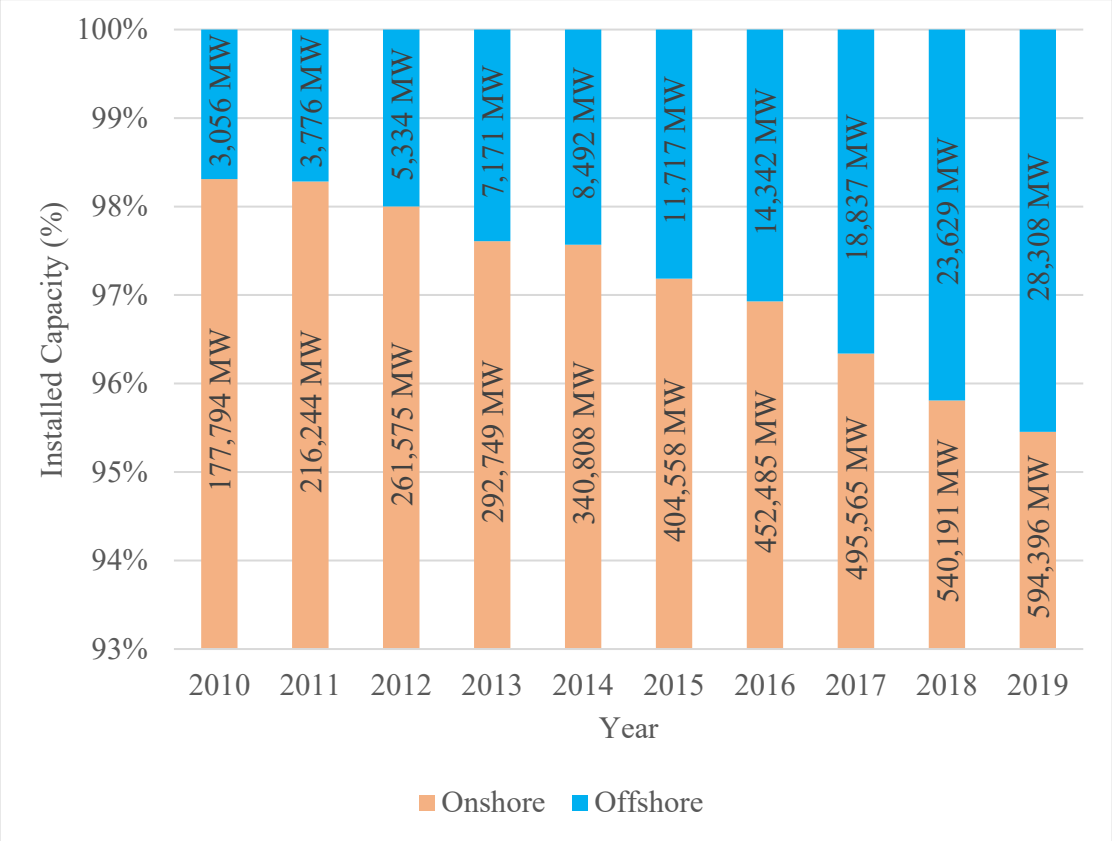

Figure 1.1 World installed wind energy capacity by year
(Source: International Renewable Energy Agency 2020)

1.1. History of Wind Turbines

Taking advantage of wind dates back to ancient history. Utilization of wind begin with the invention of the first sailing boat as early as 5000 BC. The Egyptians started to move their boats on the Nile River by taking advantage of drag force created by wind on the leather or fabric (Zafar 2018). Since then, a variety of inventions have been made to exploit wind energy and it has evolved to the present day.

The inventor of windmill is known as the Greek mathematician and engineer Heron of Alexandria, who lived in the 1st century. In the book of Heron, *Pneumatica*, the air-operated instrument named organ is designed as a pneumatic system and driven this system with a windmill (Papadopoulos 2007) in Figure 1.2 (a).

By the 10th century, Persians designed vertical windmills and used them for grinding grain and pumping water (Shepherd 1990) in Figure 1.2 (b). These ancient windmills have survived to the present day with only small deterioration and are located in the border region of Afghanistan on the territory of Iran.

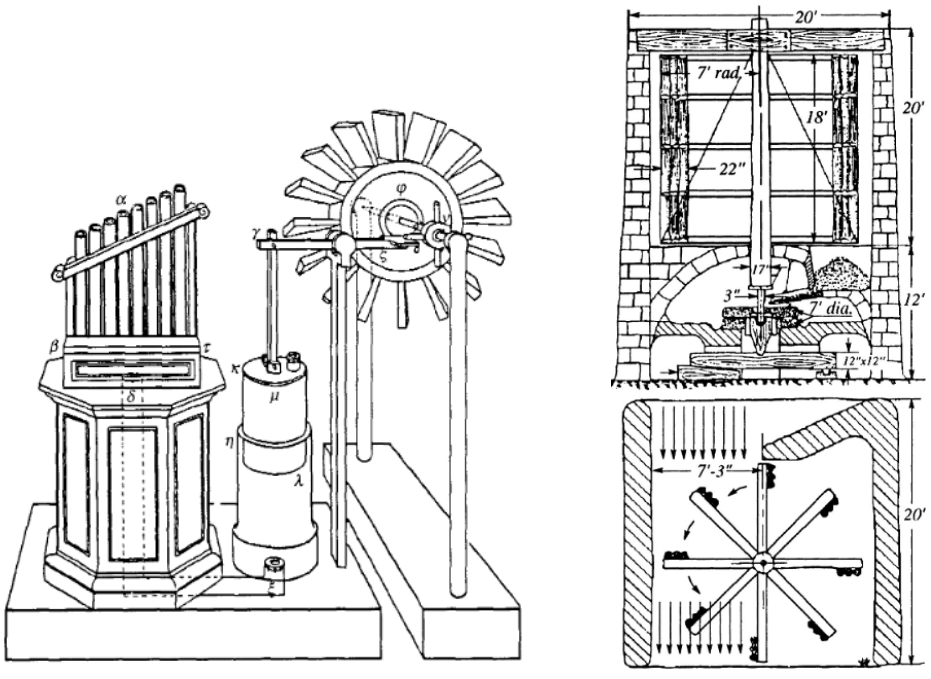

(a) (b)

Figure 1.2 History of windmill (a) Heron Design (Source: Schmidt and von Alexandria 1899), (b) Persian Design (Source: Wulff 1966)

Until 1887, various windmills were used for mechanical purposes, and the first electricity generating wind turbine was operated by Professor James Blyth at University of Strathclyde which is a humble vertical axis wind turbine. Then, first electricity generating modern and horizontal axis wind turbine (Figure 1.3) which has 12 kW power capacity was installed in Ohio by Engineer Charles Brush in 1888 (Owens 2019).

Although many breakthroughs were made on wind turbines producing electricity until 1970s, there was no serious commercial wind turbine manufacturer. But with the oil shortages that started in the 1970s, many wind turbine companies were established and wind turbines were started to be produced commercially. These developments accelerated the work done in this field.

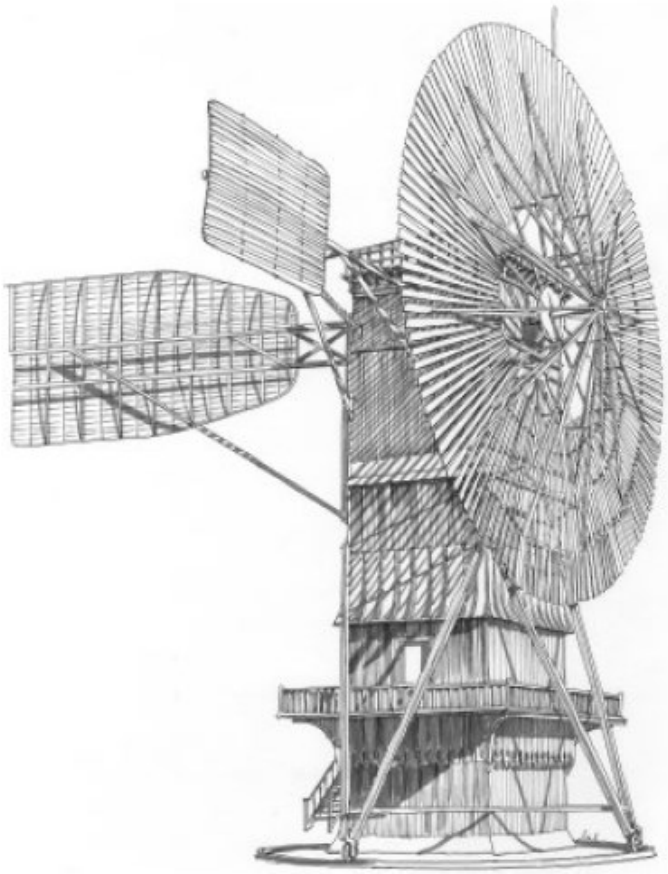

Figure 1.3 The first electicity generating horizontal axis wind turbine
(Source: Owens 2019)

Works on offshore wind studies has accelerated with the decline of economical onshore wind turbine areas and the awareness that the wind potentials offshore is higher

than the one on onshore. As a result of these studies, the first offshore wind turbine farm was installed about 2 kilometers from off the island of Lolland in Denmark in 1991. Turbines were installed on fixed types platforms because sea depth is about 5 meters in that area, (Olsen and Dyre 1993).

It was known that the potential of the wind increases as it moves away from the shore, but the sea depth also increases, therefore, after about 50m sea depth fixed types platform do not become economical anymore due to excessive tower heights. Wind turbine technology has to switch to floating types beyond the sea depths of 50m. In 2007, the first floating type offshore wind turbine which has 80kW power capacity installed as a prototype for data collection about 21 kilometers from the cost of Apulia in Italy where sea depth was about 113 meters (Busby 2012).

1.2. Characteristic Features of Wind Turbines

Turbines are produced with different characteristics according to operating and environmental conditions of the places where turbines are located. Some of the characteristic features of turbines commonly used are shown in Table 1.1. Here wind turbines are divided into two groups according to their installation locations, onshore or offshore. Also, offshore wind turbines are divided into two as floating and fixed depending on the platform types.

With respect to the rotor rotation axis, turbines are divided to two groups, horizontal and vertical. Today, the turbines used in the wind turbine industry are mostly horizontal axis wind turbines. The reason for this is that the rotors of horizontal wind turbines are positioned higher than the ground and more benefited from the wind, and the wind profiles that are higher than the ground are more uniform. On the other hand, vertical axis wind turbines are a type of turbine with small power capacity, suitable for positioning where the wind potential is variable and closer to the ground. Towers, which are the bearing elements of the turbines, are designed in accordance with the weight of the turbine that will be placed on it. The tower type used in small powerful turbine applications and windmill applications are lattice and hybrid types. Tubular shell-type tower is used in commercial turbines with large turbine weights. Rotor orientation also depends on the turbine weight. In order to avoid using yaw mechanism in small weight turbines, downwind rotor positioning is used with nacelle design, which can turn itself to the

direction of wind. In heavy and large commercial turbines, by using the upwind rotor orientation, it directly meets the wind coming on the rotor and makes more use of the wind on the rotor.

Until now, turbines with various blades have been produced, but in studies, it has been observed that the three bladed wind turbines have the most optimum efficiency with the solidity approach that best absorbs the incoming wind and explains the wind permeability of the rotor. A power regulation is done by adjusting the rotation speed of the blades at different wind speeds. The most commonly used power regulation method for large commercial turbines is based on adjusting the pitch angle of the blades. Whereas, the stall control is the preferred method for the small turbines due to its economy. There is a drive that transmits power from the rotor to the generator. The rotor can be connected to the generator with gear or it connects directly. The advantage of the direct drive system is that there is no gear friction loss, on the other hand gear connection provides more flexible rotation rate adjustment.

Table 1.1 Characteristic features of wind turbines

Axis of Rotation	• Horizontal • Vertical
Number of Blades	• One • Two • Three ...
Rotor Orientation	• Upwind • Downwind
Power Regulation	• Pitch • Stall
Power Drive Train	• Direct Drive • Gearbox • Hybrid
Tower Structure	• Tubular Shell • Lattice • Hybrid
Generator Technology	• Asynchronous • Synchronous
Platform Type (for Offshore)	• Fixed • Floating

The main components of a commonly used, three bladed, horizontal axis, upwind wind turbine is shown in the Figure 1.4. This turbine has a pitch control, a tubular shell tower structure and a gearbox.

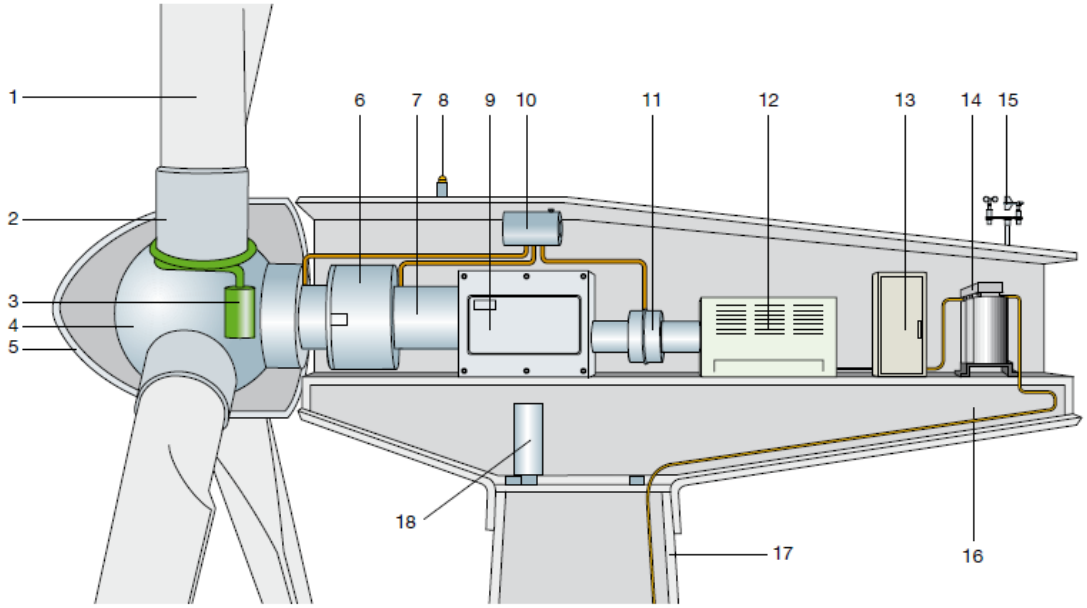

Figure 1.4 Main components of wind turbine
(Source: Tesla Institute 2020)

1. Blade
2. Blade support
3. Pitch angle actuator
4. Hub
5. Spinner
6. Main Support
7. Main Shaft
8. Aircraft warning lights
9. Gearbox
10. Mechanical breakers
11. Hydraulic cooling devices
12. Generator
13. Power converter and electric control, protection and disconnection devices
14. Anemometers
15. Transformer
16. Frame of the nacelle
17. Supporting tower
18. Yaw driving device

1.3. Offshore Wind Condition

Offshore environmental loads mainly consist of wind, wave and current interactions, and even ice floes occurring in the sea in some regions. Therefore, the designs of the turbines and platforms are made by considering that they are exposed to these effects. Profiles of wind and sea current as well as waves drawn schematically in two dimensions are shown in Figure 1.5. The current speed at sea is shown as a profile that is zero on the bottom and increases in speed as it approaches the surface of the water. Wind profile, on the other hand, has no-slip velocity on the sea surface and speedily increases with altitude. Also, the wave load is shown in the figure as a load with its own frequency and amplitude between the interaction of current and wind.

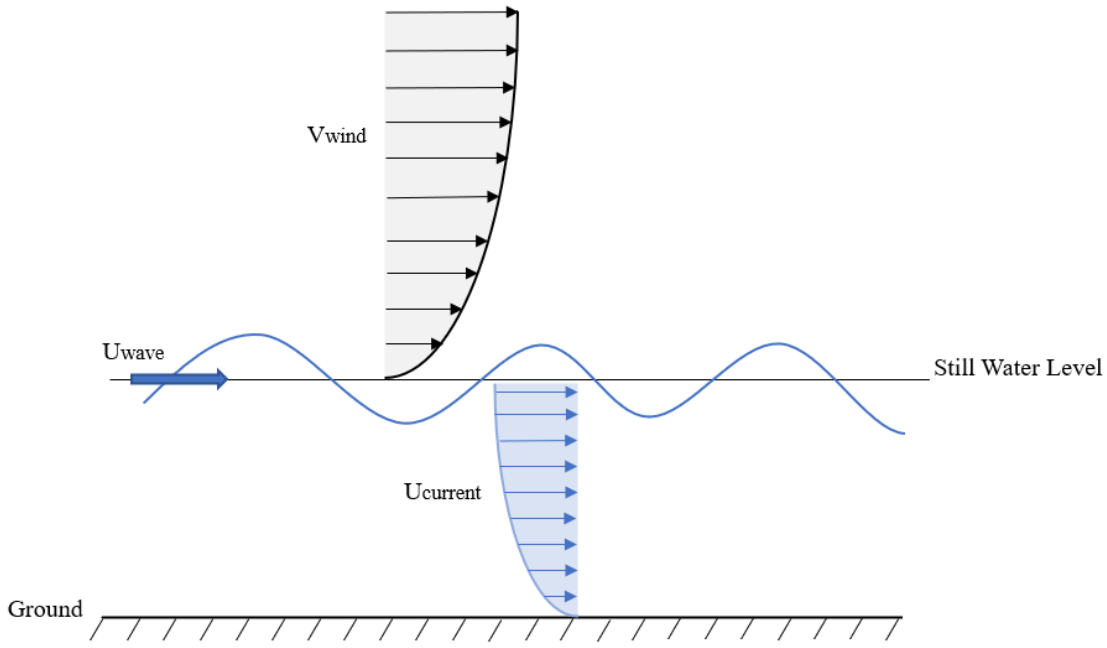

Figure 1.5 Environmental loads

Wind, wave and current loads are not necessarily in the same direction and each load affects each other. For this reason, the change of the gradient in the wind profile, the change of the gradient in the current profile, the change of frequency and amplitude of the wave depend on time and its interaction with each other.

Different roughness sources such as trees and structures on land decrease the slope of the wind profile and therefore as the roughness height increases wind energy potential

at a given height decreases. When the atmospheric boundary layers on land and at sea are compared, it is seen that the wind profile formed in the sea is more uniform and therefore its energy potential at the hub height is high. This also means that gradient of wind speed is higher. Waves formed by wind and wave interaction form a rough surface in the sea. The rough surface affects the slope of the wind profile. If the wave and wind are in the same direction, the slope of the wind profile increases, and if it is in different directions, the slope decreases (Lange et al. 2003).

Wind energy potential of a region is extracted by processing the data collected over many years with methods such as anemometers and satellites. The wind profiles, calculated, show how the atmospheric boundary layer is shaped in the region where the data is collected. Representation of a typical wind speed instantaneous distribution is shown in Figure 1.6. The differences in the actual wind speed shown in the three-dimensional profile indicate that flow is turbulent. The mean wind speed that increases according to the height shows a steep wind shear.

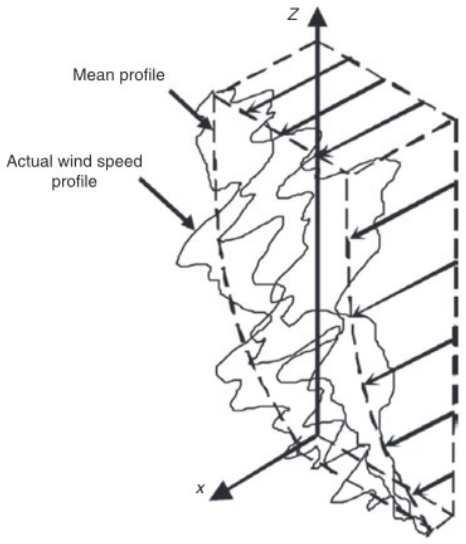

Figure 1.6 Wind profile
(Source: Tempel 2006)

In order to represent the steep changes of the wind speed, a logarithmic function used to represent the wind profile as given in Equation 1.1. This logarithmic function which was first used by Prandtl (Sutton 1937) fits nicely for most of the mean velocity profiles and allow us to predict hub level wind velocities. Nevertheless, it does not represent the wind velocity very close to the sea surface, but this does not seem to be very big obstacle for wind turbine research.

$$V(z) = V_{ref} \frac{\ln\left(\frac{z}{z_0}\right)}{\ln\left(\frac{z_{ref}}{z_0}\right)} \tag{1.1}$$

In this equation, V(z) is mean wind speed at height z, V_{ref} is mean wind speed at the reference height z_{ref} and z_0 is surface roughness length.

1.4. Types of Offshore Platforms

Offshore wind turbines and platforms are designed according to the environmental conditions where they will be located. Platforms are mainly divided into two types as fixed and floating types for use at different depths. Figure 1.7 shows the classification of the turbines according to their location and commonly used platform types. When we look at offshore turbines, it is illustrated that fixed-type platforms are used in places where sea depths are shallower than 50m's, and floating platforms are used as the sea depths are more than that (Bailey, Brookes, and Thompson 2014). This 50 meters are found by a techno-economical investigation.

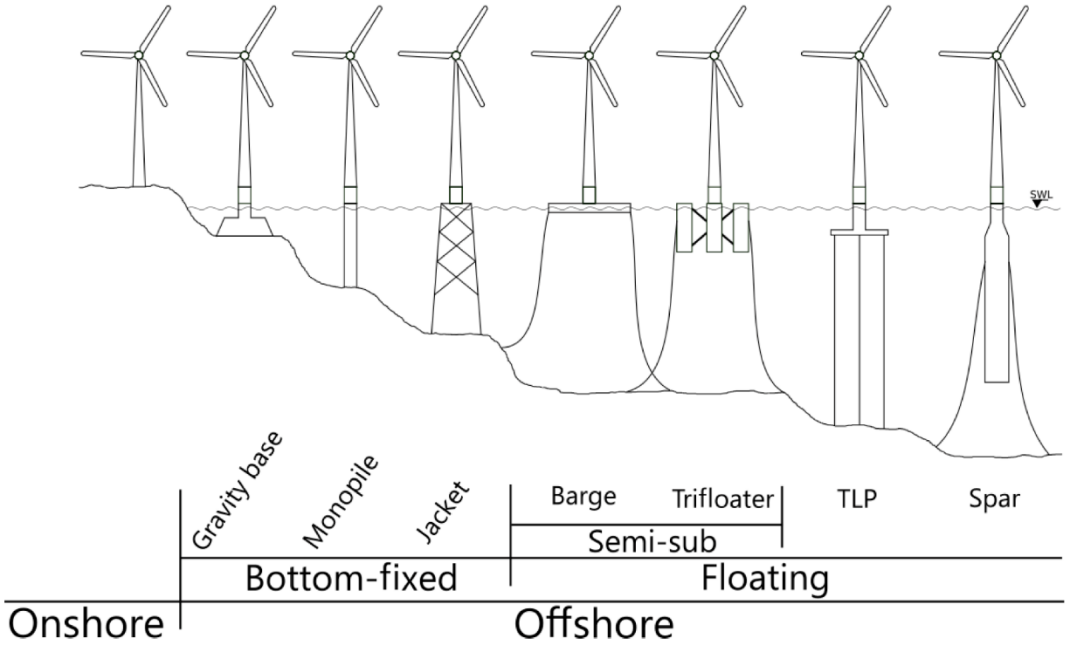

Figure 1.7 Types of platforms
(Source: Olondriz Erdozain et al. 2019)

Floating wind turbines have a handicap compared to fixed types because the platform cannot be fixed rigidly to the seabed. Located on a floating platform brings a six degree of freedom their motion and that have to be somehow limited so that a long term reliable operation can be guaranteed. There are six basic loads (Shittu et al. 2020) that affect turbine movement. These are;

- Inertia / gravitational loads
- Aerodynamic loads transferred from the rotor
    - Thrust
    - Moments
- Wind loads on the tower
- Wave loads
- Current loads
- Hydrostatic loads

Movements due to environmental loads and mechanical effects of the turbine are shown in Figure 1.8. Surge, sway and heave are the translational movements and roll, pitch and yaw movements are the rotational movements.

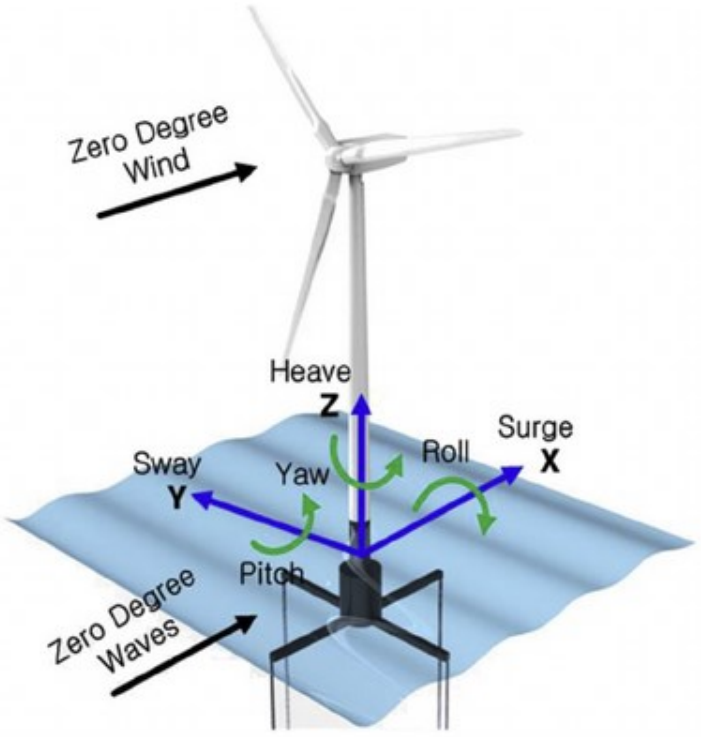

Figure 1.8 Degrees of freedom for an offshore floating wind turbine platform (Source: Tran and Kim 2016)

1.5. Motivation

Since floating wind turbines have six degrees of freedom, their oscillation and the mentioned loads become a complex problem when all loads affect each other. CFD and numerical model software are available to solve these problems, but these software are insufficient to model the whole system because they solve problem by eliminating some parameters. Therefore, the system is needed to be analyzed experimentally by modeling the floating wind turbines and environmental conditions to be analyzed in order to obtain an accurate result and improve the existing software background. The general purpose of this project is to measure the especially turbine's pitch and heave movements and to determine the forces coming to the mooring lines to which the platform is connected.

In this thesis, a commercial wind turbine is modeled and a reference model turbine is created to be used in the analysis of floating wind turbines by examining how scaling parameters are created for use in experimental studies. Also, the model wind turbine is designed for a reference wind turbine operating at 20 m/s wind speed, i.e. extreme condition. In addition, in order to create environmental conditions similar to those in nature in the laboratory environment, a wave generator is designed to simulate the wave to the wave flume in the IZTECH civil engineering hydromechanics laboratory and a wind nozzle is designed to simulate the wind. This thesis has been prepared as part of the TUBITAK project (217M451) and constitutes the initial phase of the project.

CHAPTER 2

SCALING METHODOLOGY

Experimental studies done in a laboratory with scaled down models requires full similitude of the experimental object and its environmental conditions to get accurate result. Floating wind turbines operate under two very different fluid environments at the same time, namely sea waves and atmospheric wind. This chapter presents how to combine wind/wave relationship and how to build a 1/40 scale wind turbine under these modeling conditions.

2.1. Scaling Parameters

Under aerodynamic and hydrodynamic forces, a floating wind turbine may undergo extreme swings that may negatively affect at least its performance and life expectancy and even may cause catastrophic failures. Therefore, it is necessary to predict and prevent these motions at the design stage. This is done by two separate but parallel methods; assessing the motions of the entire structure experimentally and by numerically. The reason it is required to use separate methods is to cover shortcomings of one with the other. For example, experimental methods allow us to model structure and fluid interactions for certain situations, whereas numerical techniques are flexible to try many different situations and structures but they are needed to be assured by some experimental results. Numerical methods are done by hydrodynamical and aerodynamical simulation of the entire structure (floating platform and wind turbine), but those models contain many simplifications and assumptions that may not represent the reality. Therefore, experiments are found to be necessary to assess some critical the dynamics of the structure. Majority of experimental tests have to use economical scaled models where it is necessary to establish similarity so that the model scale motions represents the full scale. Concept of dimensional analysis is needed to achieve similarity and it is defined under three main headings (Çengel and Cimbala 2010).

- Geometric Similarity; the model must have the same shape as the prototype
- Kinematic Similarity; the velocities at any point in the model must have the same direction and location as the prototype
- Dynamic Similarity; all forces scaled nondimensionally must match at the model and the prototype

Geometric similarity can be considered as using a single length-scale for size reduction process which results in a single ratio for corresponding lengths. Kinematic similarity, on the other hand, can be considered as using a single time-scale which results in a single ratio for corresponding velocities. But the prerequisite for providing kinematic similarity is to obtain geometric similarity first. In addition, dynamic similarities are based on the principle of dimensionless simulation of forces, and kinematic similarity has to be satisfied first to achieve dynamic similarity. In order to achieve these three principles, the following dimensionless parameters are formally obtained by *Buckingham Pi* theorem.

The scale factor is defined as the ratio between prototype and model parameter, which is indicated λ. Also, the application of this scale factor on the characteristic length provides geometric similarity.

$$\lambda = \frac{P_m}{P_p} \tag{2.1}$$

Hydrodynamic and aerodynamics forces can be scaled with Froude and Reynolds numbers, respectively. Froude number is a ratio of inertial and gravitational forces and that dimensionless number provides dynamic similarity. Froude number is usually used scale forces created by gravity driven surface waves.

$$Fr = \frac{U}{\sqrt{gL}} \tag{2.2}$$

where, U is fluid velocity, g is gravitational acceleration and L is characteristic length.

Reynolds number is used to scale forces that originates from formation of boundary layers. Therefore, Reynolds number is given as a ratio of inertial and viscous forces. This dimensionless number provides dynamic similarity.

$$Re = \frac{UL}{\nu} \tag{2.3}$$

where, U is fluid velocity, L is characteristic length and ν is kinematic viscosity.

Another aerodynamic parameter that must be matched is the Tip Speed Ratio of the blades. This dimensionless number provide kinematic similarity. TSR is computed as,

$$TSR = \frac{\Omega R}{U} \tag{2.4}$$

where, Ω is the rotor rotational speed, R is the blade tip radius and U is the wind inflow velocity. This ratio has to be kept constant from prototype to scale model so that the wake spiral of the tip vortices will be similar. Besides the lift and drag coefficients, if TSR is kept the same then, thrust and power coefficients is expected to be scaled correctly.

Froude scaling is very suitable for wave flume experiments and also Reynolds scaling is applicable for aerodynamic experiments. Unfortunately, it is not possible to apply simultaneously Froude and Reynolds scaling (Gueydon and Fernandes 2013) under the same viscosity and gravitational fields assumptions. Impossibility of satisfying both scaling parameters can simply be seen as

Froude Number Scaling	Reynolds Number Scaling
$Fr_p = Fr_m$	$Re_p = Re_m$
$\frac{U_p}{\sqrt{gL_p}} = \frac{U_m}{\sqrt{gL_m}}$	$\frac{U_p L_p}{\nu_p} = \frac{U_m L_m}{\nu_m}$
$U_m = U_p \sqrt{\frac{L_m}{L_p}}$	$U_m = U_p \frac{L_p}{L_m}$

$$U_m^{Fr} \neq U_m^{Re} \tag{2.5}$$

where, the indices p and indices m represent prototype and model, respectively. Usually, Froude scaling have to be used for model scaling of floating wind turbines because the majority of the forces that cause serious swings of the platforms comes from sea waves.

2.1.1. Reynolds Number Discrepancy

Satisfying only the Froude number creates very small Reynolds numbers. On the air side of a floating wind turbine majority of the aerodynamical forces come from the blades themselves compared to the forces on tower and the nacelle (Rommel, Di Maio, and Tinga 2020). Basic forces in aerodynamics such as drag and lift on the airfoil depend on the Reynolds number and these forces determine the overall aerodynamic properties and performance of the turbine. Drag and lift force are defined as the projection of the total force, that comes on an airfoil, on the direction of the mean wind speed and perpendicular to it respectively, see Figure 2.1. Since Reynolds number is not matched at all, lift and drag forces have to be scaled by chancing the aerodynamic shapes. Even then, it is almost impossible to match both of them. Since the drag forces are much dominant in extreme wind conditions, in this study only drag forces were tried to be matched, due to this Reynolds discrepancy.

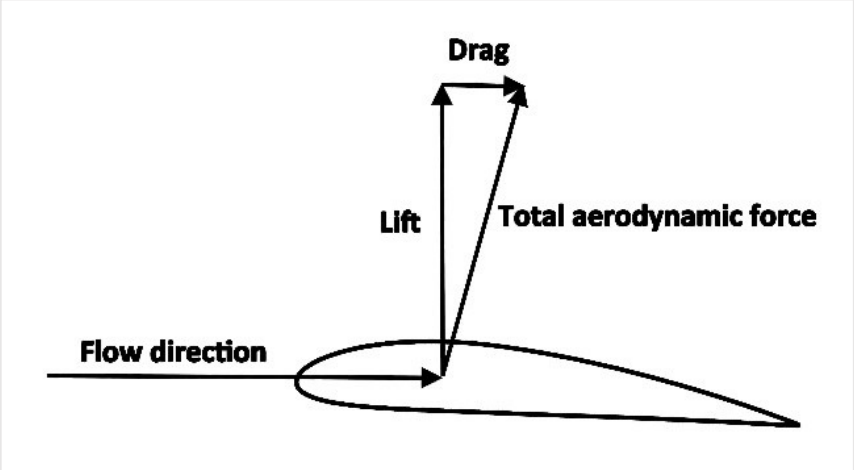

Figure 2.1 Airfoil basic forces

Since a system where hydrodynamic forces are dominant is modelled, Froude number similitude have to be used. According to Froude number, length scale factor and velocity scale factor defined as λ_L and λ_V, respectively.

$$\lambda_L = \frac{L_p}{L_m} \tag{2.6}$$

$$\lambda_V = \sqrt{\frac{L_p}{L_m}} \tag{2.7}$$

Froude dimensional scaling factors are applied on Reynolds number and a new Reynolds number scaling factor is defined in order to show Reynolds number relation between the model and the prototype airfoils. This ratio grows as the scaling factor goes up.

$$\lambda_{Re} = \lambda_L \lambda_V = (\lambda_L)^{3/2} \tag{2.8}$$

In this study, Northel's P36/300 wind turbine is used as a reference turbine. This turbine uses NACA4415 (Figure 2.2) type airfoil profile on the blade where it has the most impact on power generation on the turbine blade.

The tower height and rotor diameter of the reference wind turbine are 36 meters. Therefore, scaling ratio is selected as $\lambda_L=L_p/L_m=40$ which is the smallest possible scale factor that could be used in the wave flume in the Civil Engineering Hydromechanics laboratory of IZTECH. This wave flume has 1m width, 1.40m depth and 1m water depth. Then, Reynolds scaling factor is obtained as $\lambda_{Re}=(\lambda_L)^{3/2}=252.98$ from equation 2.8 to calculate Reynolds relation between prototype and model airfoils.

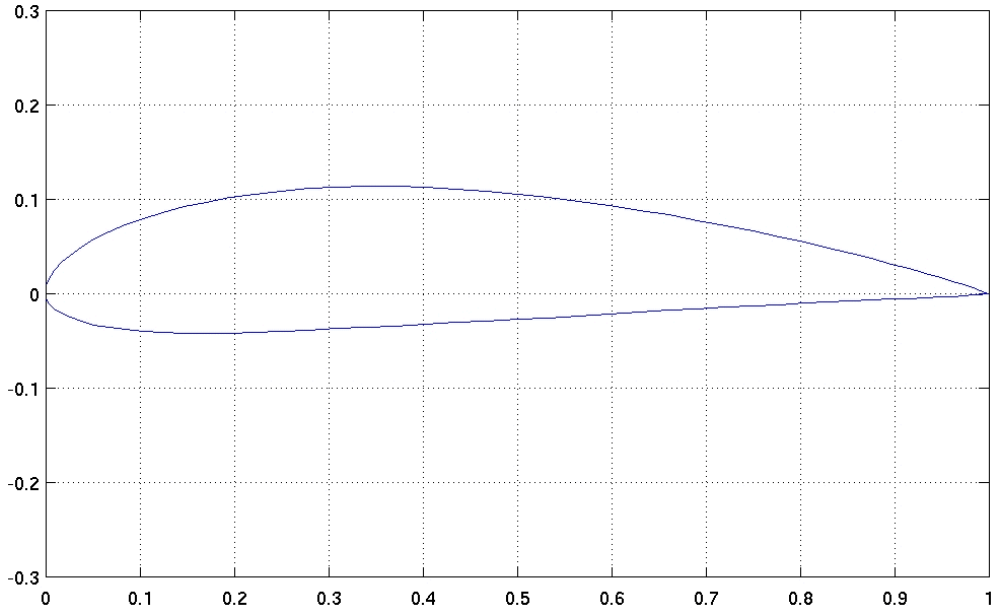

Figure 2.2 NACA4415 Airfoil
(Source: UIUC Applied Aerodynamics Group 2020)

Model blade selection has to be designed in a way that it has similar as possible lift and drag coefficients so that the aerodynamical forces modelled correctly. The lift and drag coefficients of prototype turbine blade section, NACA4415, is numerically analyzed by using XFOIL software (Drela 1989) which allows viscous-inviscid coupling. Analyses give lift and drag force coefficients with respect to angle of attack as seen in Figure 2.3.

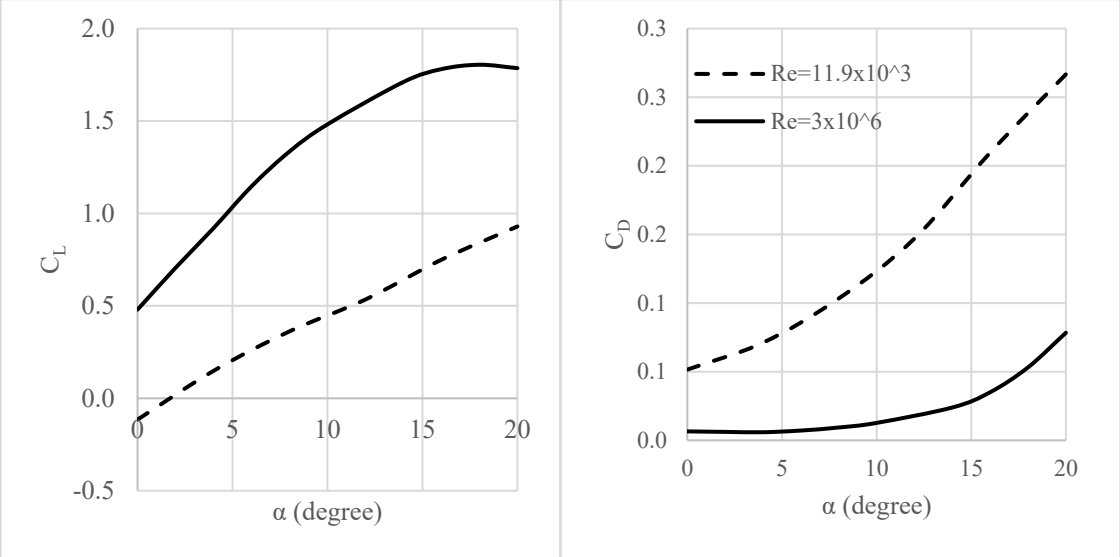

Figure 2.3 Lift and drag coefficient as a function of angle of attack for NACA4415 airfoil at different Reynolds numbers.

As seen in the graphs, there are obvious differences between the coefficients in the simulation using Reynolds scaling factor. Therefore, Reynolds similitude cannot be used in a strict sense and this is how Reynolds discrepancy show itself. On the other hand, similar lift and drag coefficients can be obtained by using a different airfoil profiles. This technique usually allows a limited agreement, nevertheless, it is better than nothing.

2.1.2. Froude Scaling and Tip Speed Ratio Similitude

Froude number scaling is used for platform geometric scaling and wave scaling because of the importance of the hydrodynamic parameters. Therefore, Froude number for free surface waves,

$$Fr_{wave} = \frac{C}{\sqrt{gL}} \tag{2.9}$$

where, C is the wave celerity (a.k.a. phase speed), or propagation speed, g is the local acceleration due to gravity and L is the characteristic length.

Froude number scaled wind is applied for creating wind profile because of Reynolds discrepancy. For this reason, Froude number for wind scaling is given Equation 2.10. In order to make an accurate assessment of experimental results and to establish a relationship between the experiments, a relationship must be developed between the wind speed and wave celerity that forms two different Froude numbers. This relation is defined as ratio of parameters and named as Q that is given in Equation 2.11.

$$Fr_{wind} = \frac{U}{\sqrt{gL}} \tag{2.10}$$

where, U is the wind speed, g is the gravitational acceleration and L is the characteristic length.

$$Q = \frac{U}{C} \tag{2.11}$$

Q must be kept constant at different experimental conditions so that the Froude scaling works for the model.

In summary, scaling should be provided based on two main equations. Dynamic similarity is achieved by using Froude number. In addition, kinematic similarity is achieved by using TSR.

$$Fr_p = Fr_m \tag{2.12}$$

$$TSR_p = TSR_m \tag{2.13}$$

Based on the explained equations to be used, scaling factors can be obtained as a result of unit analysis in Table 2.1. Also, additional parameters and information can be found in Offshore Structure Modelling book (Chakrabarti 1994).

It is necessary to explain the main reason why the scaling factor is chosen as 1/40. A large as possible scaling ratio is desired because the size effects on the measured values will be minimized. And therefore, the weight, power and thrust force values will be higher and as a result, easier to measure. On the other hand, there are restrictions due to the dimensions of the wave flume, and a larger model turbine cannot be installed in it, therefore, a scale ratio that is just big enough for the wave flume allows must be selected.

Table 2.1 Scale factors of parametes

Parameter	Unit	Scale Factor
Length	[L]	λ
Area	$[L]^2$	λ^2
Volume	$[L]^3$	λ^3
Density	$[M][L]^{-3}$	1
Mass	[M]	λ^3
Time	[T]	$\lambda^{0.5}$
Frequency	$[T]^{-1}$	$\lambda^{-0.5}$
Velocity	$[L][T]^{-1}$	$\lambda^{0.5}$
Acceleration	$[L][T]^{-2}$	1
Force	$[M][L][T]^{-2}$	λ^3
Moment	$[M][L]^2[T]^{-2}$	λ^4
Power	$[M][L]^2[T]^{-3}$	$\lambda^{3.5}$
Stress	$[M][L]^{-1}[T]^{-2}$	λ
Mass moment of inertia	$[M][L]^2$	λ^5
Area moment of inertia	$[L]^4$	λ^4

CHAPTER 3

APPLICATION OF SCALING METHODOLOGY

As scaling methodology is mentioned in the previous chapter, it is obvious that wind turbine blade cannot be scaled completely when the scaling factor is too big and therefore Reynolds numbers cannot be matched which is the case for offshore wind turbines. Some sample scaling factors of floating wind turbine rotors used in similar studies are listed in the Table 3.1 as a reference. As it seen in this table scaling factors used very large ratios in which Reynolds number matching is impossible to achieve.

Table 3.1 Scaling studies

Study Number	Turbine Power	Scaling Factor	Rotor Model
1	2.4MW	1/150	disc with holes
2	10MW	1/105	drag disc
3	5MW	1/60	concentrated mass
4	6MW	1/40	ducted fan
5	5MW	1/50	geometric scaled
6	10MW	1/75	thrust and power scaled

In the first study by Ishihara et al. (2007), a disc with perforated holes is used to model the thrust force in which only thrust coefficients are matched. In the second study, the thrust force is modelled using a scaled rotor diameter disc (Cermelli, Roddier, and Aubault 2009). In the third study, rotor is not used and only the center of gravity of the turbine is modelled (Guanche et al. 2014) where study of the effect of only mass on oscillation is aimed to be modelled. In the fourth study, a fan generating thrust force is placed on the tower (Azcona et al. 2014) where again the thrust forces are scaled. In the fifth study, a geometrically scaled rotor is used, but the desired thrust force and power are not obtained (Martin 2011) due to the very reasons of large scaling factor effect we have explained earlier. In the sixth study, by changing blade profile, a new blade is created with Froude scaling and aeroelastic optimization, power and thrust force are scaled (Bayati et al. 2017).

In this section, firstly Blade Element Momentum Theory (BEMT) is explained to perform rotor aerodynamic analysis. Prototype wind turbine selected is called Poyra P36/300 which is made by Northel Company. Its properties are explained and analyzed to validate company data with this theory. Then, using scaling methodology described, thrust scaled model of the wind turbine blade and turbine are explained.

3.1. Blade Element Momentum Theory

Blade element momentum is a theory created by combining the method called actuator disk theory or momentum theory with blade element theory. It is first used in by Froude as his blade element momentum theory (1878), later it is modified and revised by Glauert (1926) (Branlard 2017). Blade element momentum theory (BEMT) is one of the widely used methods today because it is a simple theory and gives correct enough results in preliminary design and analysis.

Actuator disc theory is obtained only by creating 1D axial momentum equation, conservation of mass and Bernoulli equation. The pressure and velocity differences that occur are shown in Figure 3.1. According to the Bernoulli principle, the free stream encounters a blocking effect on the disc, where the speed decreases and the pressure increases. Since the disc is fixed, negative pressure is created behind it and it is equalized to atmospheric pressure as it moves away. Due to these effects of flow and pressure, the stream tube is formed in an expanding way.

Also, in this theory, an axial induction factor is defined and given in Equation 3.1, which defines the relationship between the velocity differences in disk and free stream.

$$a = \frac{U_\infty - U_d}{U_\infty} \tag{3.1}$$

where, U_∞ is free stream velocity and U_d is velocity at disk. It is known that the flow velocity at the disk is the average of wake and free stream velocity. Therefore, the relationship between free stream and wake velocities can also be defined with the axial induction factor in Equation 3.2.

$$U_W = U_\infty(1 - 2a) \tag{3.2}$$

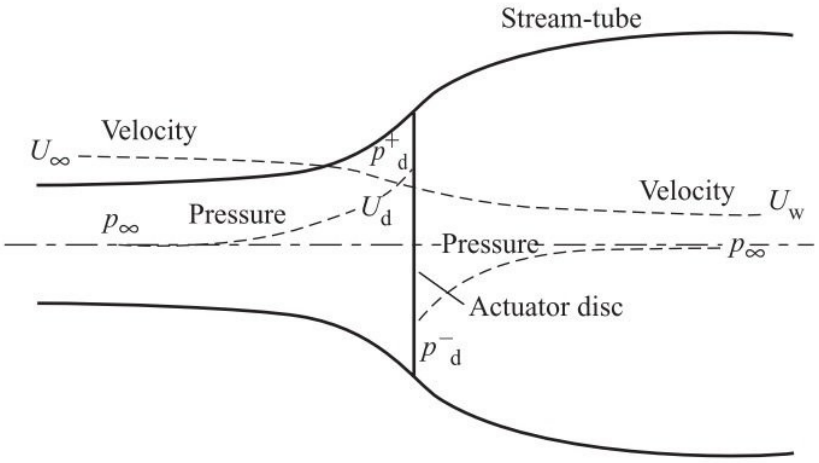

Figure 3.1 Representation of momentum theory
(Source: Quinn, Schepers, and Bulder 2016)

Blade element theory is based on the calculation of the forces on the airfoil in each section by dividing the blade into an infinite number of sections (Figure 3.2). Also, in this theory, a tangential induction factor is defined and given in Equation 3.3, which defines the relationship between the rotational speed of airfoil and tangential velocity at wake.

$$a' = \frac{\omega}{2\Omega} \tag{3.3}$$

where, ω is tangential wake velocity and Ω is angular speed of blade cross-section.

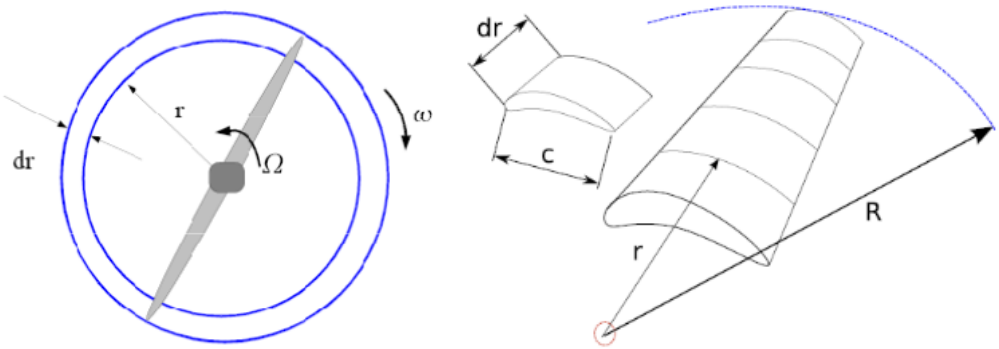

(a) (b)

Figure 3.2 Blade element theory (a) Stream tube (b) Blade sections
(Source: Kulunk and Yilmaz 2009)

The BEMT algorithm is a theory created by combining described the momentum theory and the blade element method. This theory also defined a sectional or local tip speed ratio, which is performance determining factor.

$$\lambda_{TSR} = \frac{\Omega r}{U_\infty} \tag{3.4}$$

where, Ω is angular speed, r is sectional radius from center of hub and U_∞ is tangential inflow velocity.

First known data in BEMT algorithm are the number of blades, axial inflow velocity, rotor radius, and rotational speed. But there are two important values to know here, these are the axial velocity and the tangential wake velocity on the blade. These velocities form the relative velocity coming on the airfoil in the blade section, and the lift and drag forces of the airfoil can be calculated from the relative velocity. Therefore, induction factors are initially considered to be zero, then relative velocity and angle of attack are calculated. Tangential and normal force coefficients are calculated from the C_L and C_D values formed in the airfoil, and induction factors are checked again. These processes continue until the induction factors converge. Detailed information about the theory can be obtained from Branlard's book (Branlard 2017).

The thrust and power coefficients obtained as a result of BEMT application, which is an iterative method, are given in equation 3.5 and 3.6.

$$C_T = \frac{2}{R^2}\int_{r_{hub}}^{R} r C_t(r) dr \tag{3.5}$$

$$C_P = \frac{2}{R^2}\int_{r_{hub}}^{R} r \lambda_{TSR} C_q(r) dr \tag{3.6}$$

where, R is blade length, r is blade section length, C_t is local thrust coefficient, C_q is local torque coefficient and λ_{TSR} is local tip speed ratio.

In this study, QBlade (Marten et al. 2013) open-source, cross-platform simulation software based on BEMT is used. Flow chart that explains working principle of QBlade is shown in Figure 3.3. Some of the correction factors used in this software are i- Prandtl tip and root loss correction, ii- 3D flow correction, iii- Reynolds drag correction and iv- Foil interpolation.

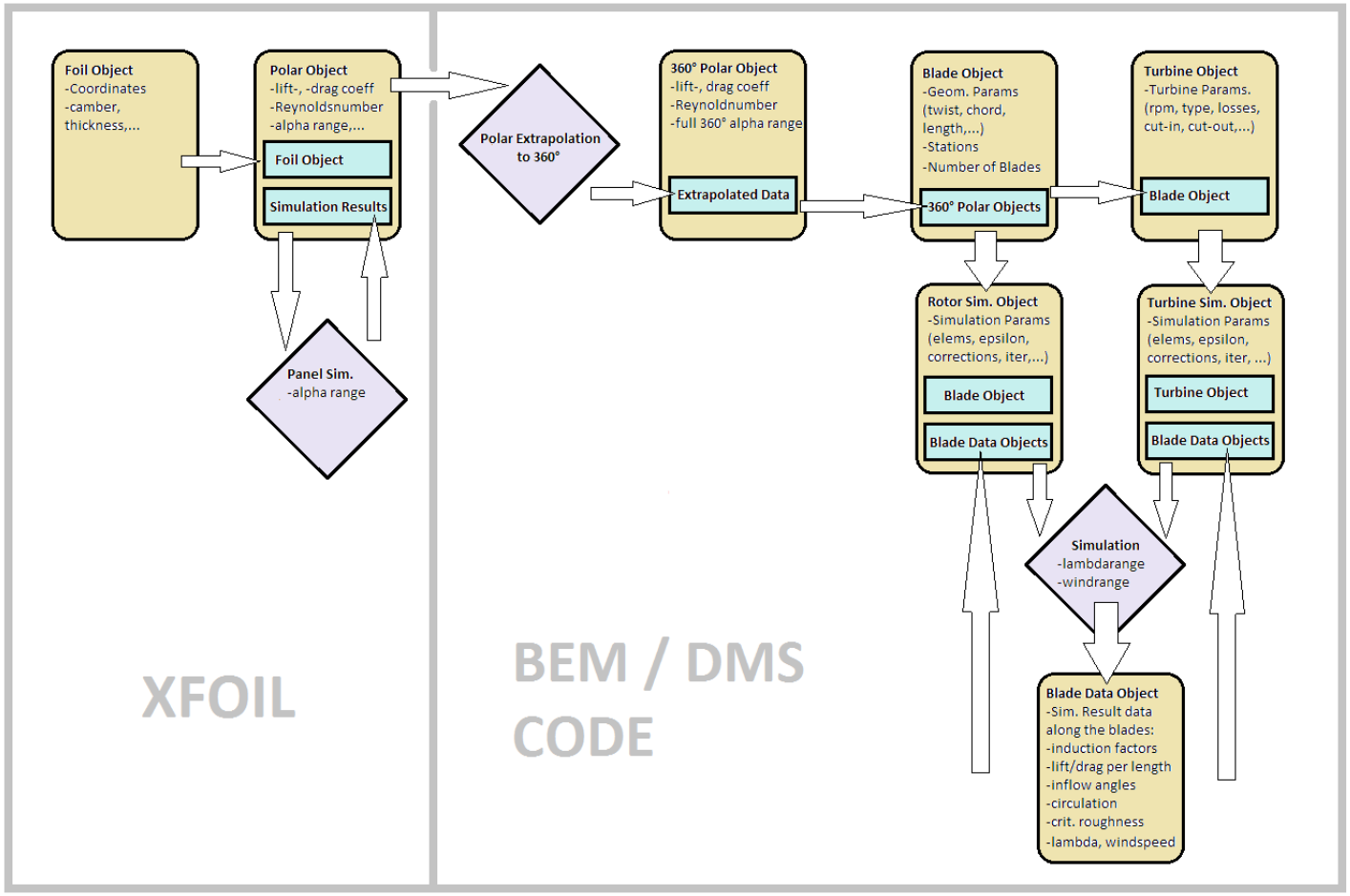

Figure 3.3 Data objects and data flow in QBlade
(Source: Marten and Peukert 2013)

3.2. Analysis of Reference Wind Turbine Rotor

Northel POYRA P36/300 wind turbine is used as a reference and the blades of this wind turbine have a blade geometry consisting of a total of 8 different airfoils derived from NACA4415 airfoil. Turbine rotor and blade specifications with operating conditions are given in Table 3.2.

Table 3.2 Northel POYRA P36/300 turbine spesifications

Parameter	**Description**
Number of blades	3 bladed
Hub diameter	2 meters
Rotor diameter	36 meters
Cut in wind speed	2.9 m/s
Cut out wind speed	25 m/s
Minimum rotor speed	15 rpm
Maximum rotor speed	50 rpm
Turbine power	320 kW
Power regulation	Pitch control

The results of QBlade analysis are given in the graphics below.

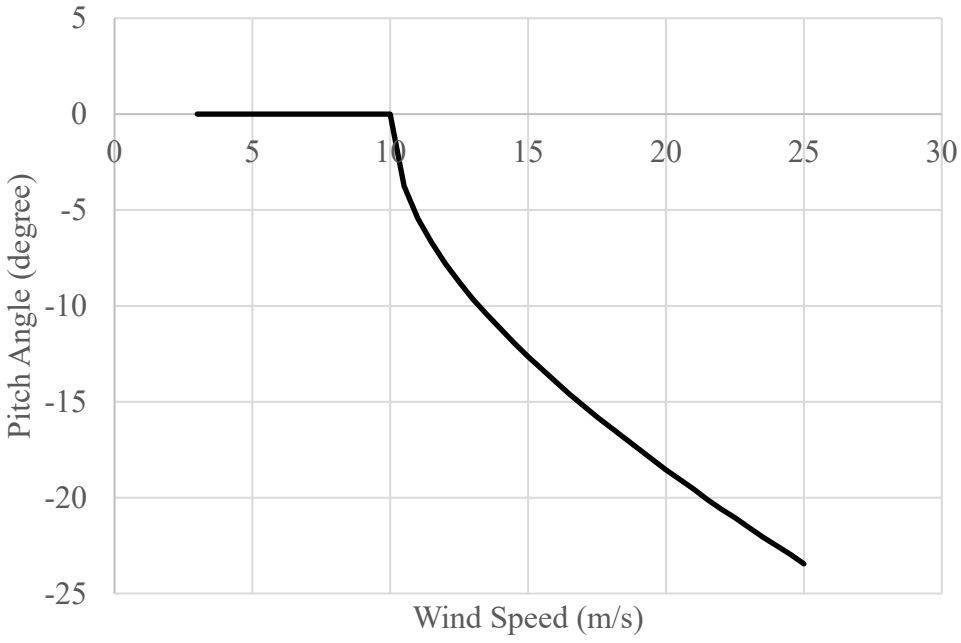

Figure 3.4 Pitch angles with respect to wind speeds

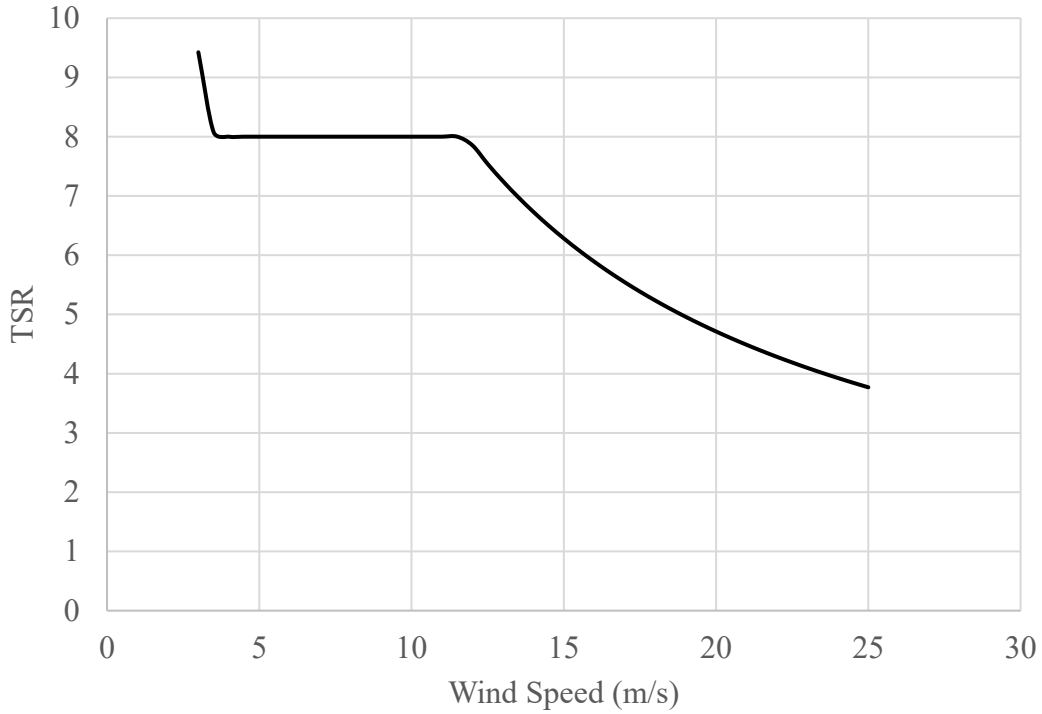

Figure 3.5 Tip speed ratio with respect to wind speed

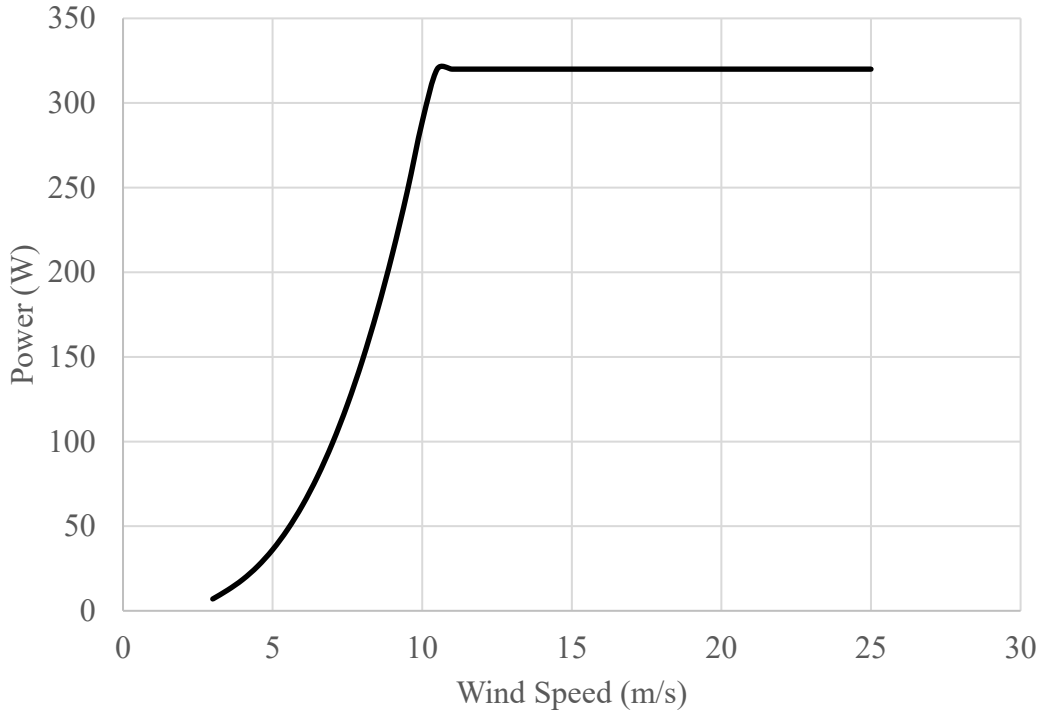

Figure 3.6 Power with respect to wind speed

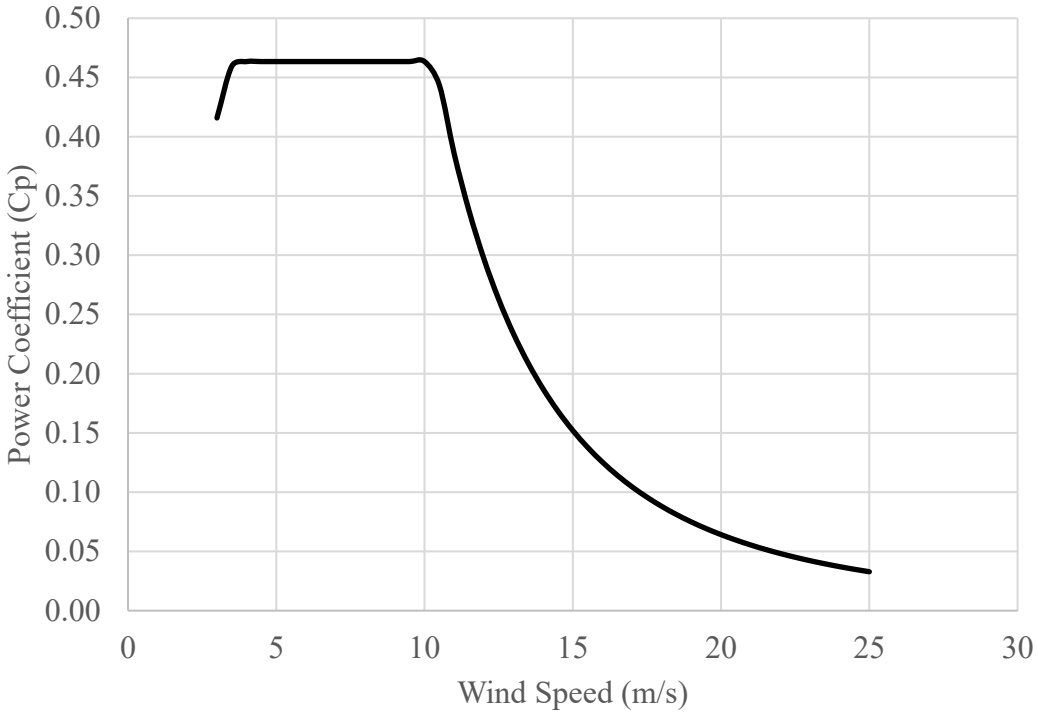

Figure 3.7 Power coefficient with respect to wind speed

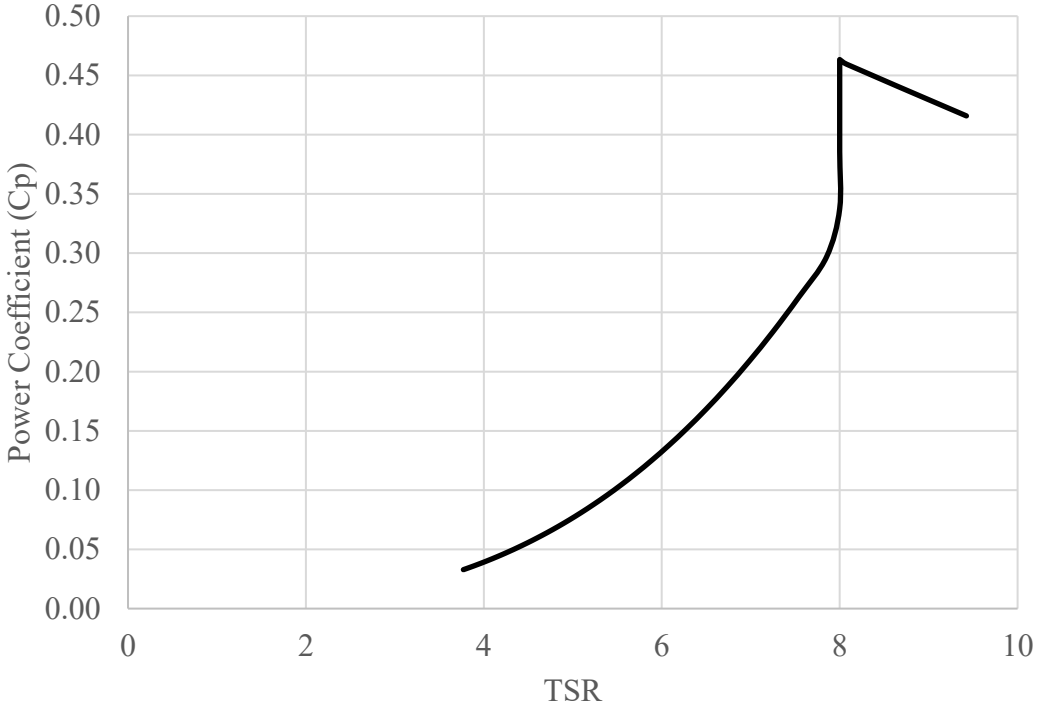

Figure 3.8 Power coefficient with respect to tip speed ratio

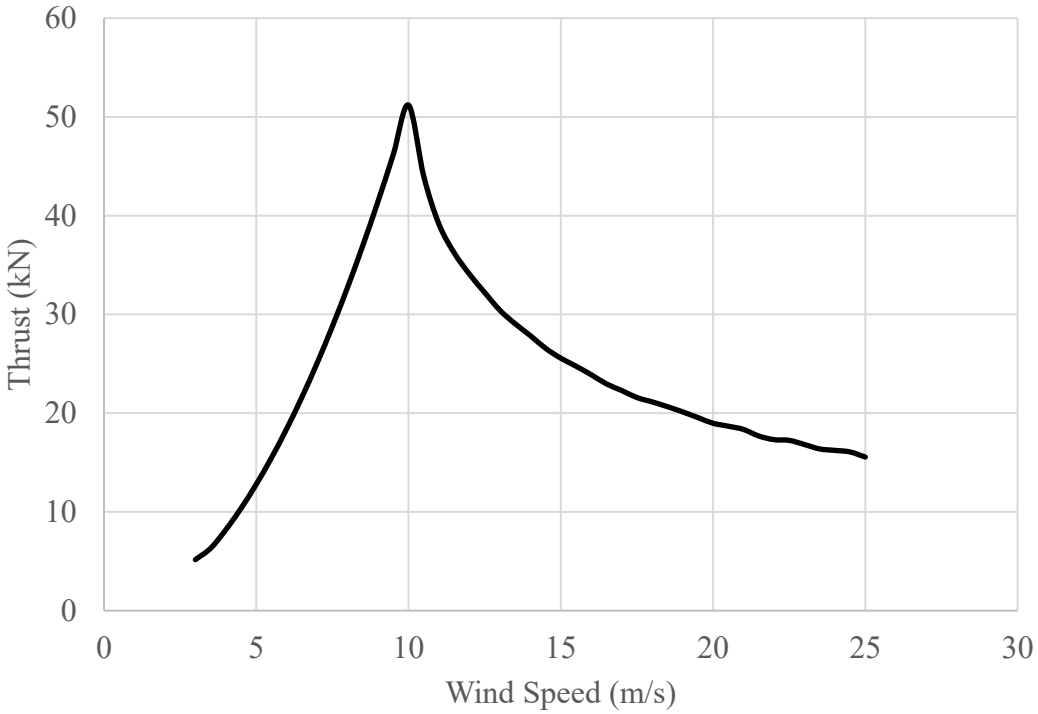

Figure 3.9 Thrust force with respect to wind speed

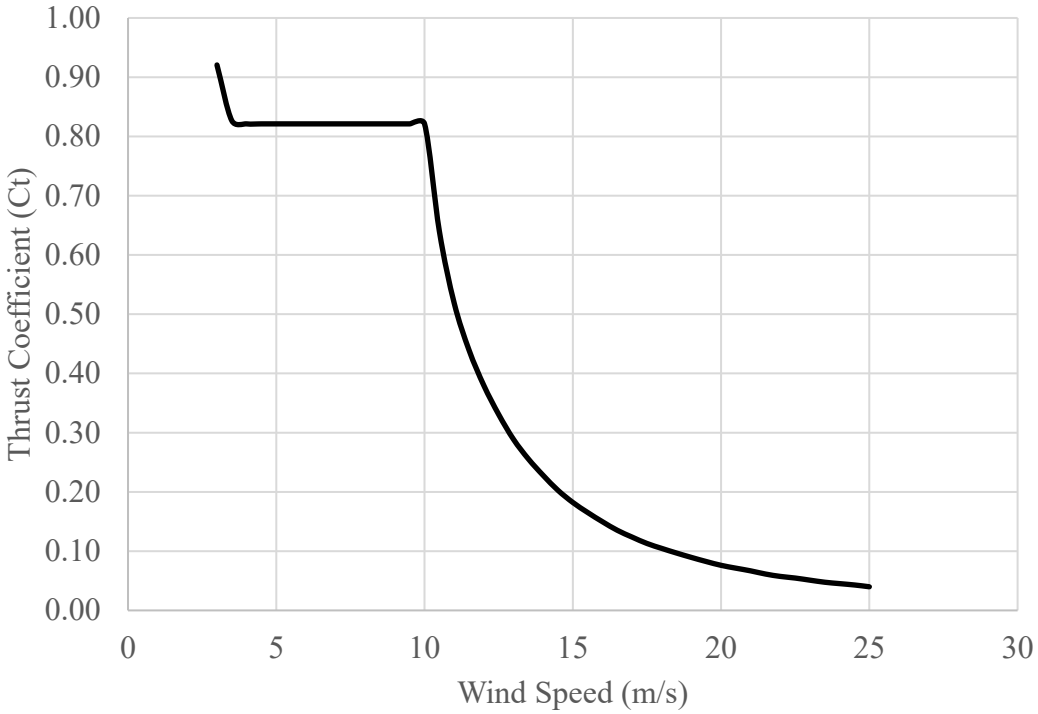

Figure 3.10 Thrust coefficient with respect to wind speed

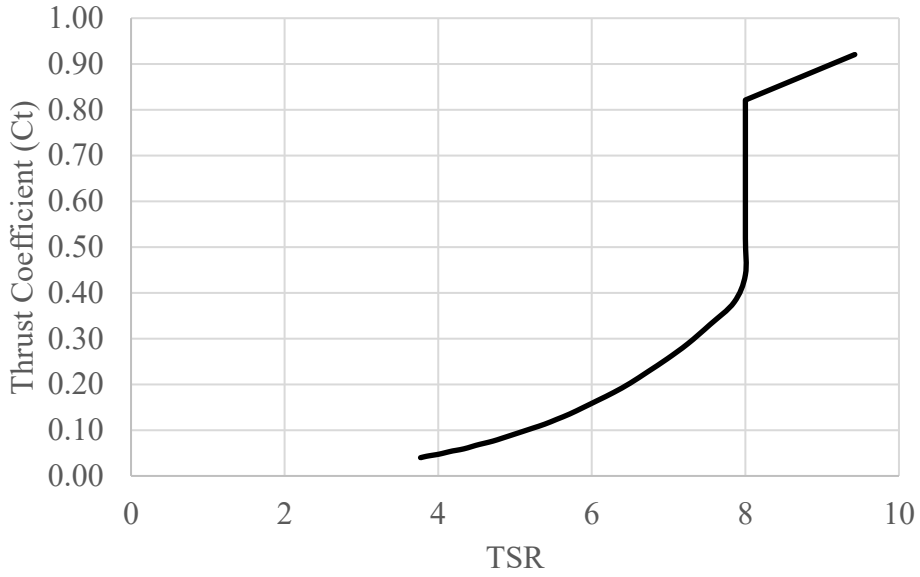

Figure 3.11 Thrust coefficient with respect to tip speed ratio

It is important at which wind speeds the pitch control is activated and is helpful in interpreting the graphics. In order to interpret the results of the analysis, it is necessary to specify the explicit equations of total Thrust coefficient, power coefficient and tip speed ratio.

$$C_T = \frac{T}{\frac{1}{2}\rho A_d U_\infty^2} \tag{3.7}$$

$$C_P = \frac{P}{\frac{1}{2}\rho A_d U_\infty^3} \tag{3.8}$$

$$TSR = \frac{\Omega R}{U_\infty} \tag{3.9}$$

where, T is thrust force, P is power, ρ is air density, A_d is rotor area, Ω is angular speed, R is rotor radius and U_∞ is inflow velocity.

In Figure 3.4, we can observe that pitch control is not performed until the wind speed reaches 10 m / s and after this speed it increases to an increasing angle. The reason for this is to fix the rotor rotation speed and keep the generated power constant.

In Figure 3.6, it is observed that the power increases until it reaches a wind speed of 10 m / s, after this speed it remains at a constant power with pitch control. In Figure

3.7, the power coefficient increased from 2.9 m / s to 4 m / s wind speed and remained steady up to 10 m / s, gradually decreasing after 10 m / s wind speed, which is clearly seen when looking at Equation 3.8, the wind speed while increasing, the power remains constant. In Figure 3.8, TSR is the highest number at low wind speeds, and it appears that the power coefficient decreases as the wind speed increases.

Figure 3.9 shows the change of thrust force according to the wind speed. Thrust force increased up to 10 m / s wind speed and decreased gradually after this speed, because the pitch control is activated at 10m / s. In Figure 3.10, thrust coefficient decreased from 2.9 m / s to 4 m / s wind speed and continued steadily up to 10 m / s. The wind speed continued to increase while the thrust force decreased after 10 m / s wind speed, and the graph showed a downward trend, which can be explained by equation 3.7. In Figure 3.11, TSR is the highest number at low wind speeds, and it appears that the thrust coefficient decreases as the wind speed increases.

3.3. Design of Model Blade

The model blade and rotor design parameters are found by using the 1/40 scaling factor and the thrust force of the turbine at 20 m/s operating conditions. The desired power parameter cannot be modeled because the model rotor diameter and revolution are insufficient to produce any reliable power output.

Table 3.3 Desired model rotor spesification

Parameters	**Reference**	**Scaling Factor**	**Model**
Hub diameter	2 meters	λ	0.05 meters
Rotor diameter	36 meters	λ	0.9 meters
Wind speed	20 m/s	$\lambda^{0.5}$	3.16 m/s
Rotor speed	50 rpm	$\lambda^{-0.5}$	316.22 rpm
Power	320 kW	$\lambda^{3.5}$	0.79 W
Power coefficient	0.064	1	0.064
Thrust	18.9 kN	λ^{3}	0.296 N
Thrust coefficient	0.076	1	0.076
Blade mass	1774 kg	λ^{3}	27.72 gr

In rotor modelling study, it is tried to obtain the desired thrust force with manual (try-and-error) blade design. Many low-Reynolds airfoils existing in the University of Illinois airfoil database and many flat plate airfoil types created with JavaFoil (Hepperle 2018) software are considered and tried with QBlade.

In this study, modelling is done assuming rigid body blades and a tower. Nevertheless, a strength analysis is made for the blades since they will need to build very light and they are needed to operate under rotational rates excess 350 rpm. In some of the blade designs, ABS plastic is chosen as the material and the deflection is observed to be excessive in structural analysis. In addition, it is observed that the desired blade mass cannot be obtained. Therefore, it is soon observed that the desired model blade design has to depend on three main criteria and chord width must be created with these criteria; they are i- Material selection, ii- Production method, iii- Desired mass.

3.3.1. Design Algorithm

In order to explain the design algorithm, first of all, it is necessary to understand the velocity vectors and angles that occur on a typical 2D cross-section of a wind turbine blade (Figure 3.12). Here, the loads occurring in the blade section are; F_N is the normal force in the direction of the incoming wind, F_T is the tangential force in the direction of rotation of the blade, F_L and F_D are the lift and drag forces. In these forces, tangential and normal forces are perpendicular to each other, lifting and drag forces are also perpendicular to each other. It was stated that the induction factors were used to determine the velocities on the blade section. As it can be seen from this image, a relative velocity vector (W) can be constructed by considering wind speed (axial), rotational speeds (tangential) and related induction factors. The angle formed between the relative velocity vector and the blade rotation axis is called the inflow angle (ϕ). The angle between the airfoil chord line and the relative velocity vector is known as the angle of attack (AoA). Also, the angle between the rotor plane axis and the chord line is defined as the sectional pitch angle (θ_p) which consists of blade pitch angle at the tip (β) and blade twist angle (θ).

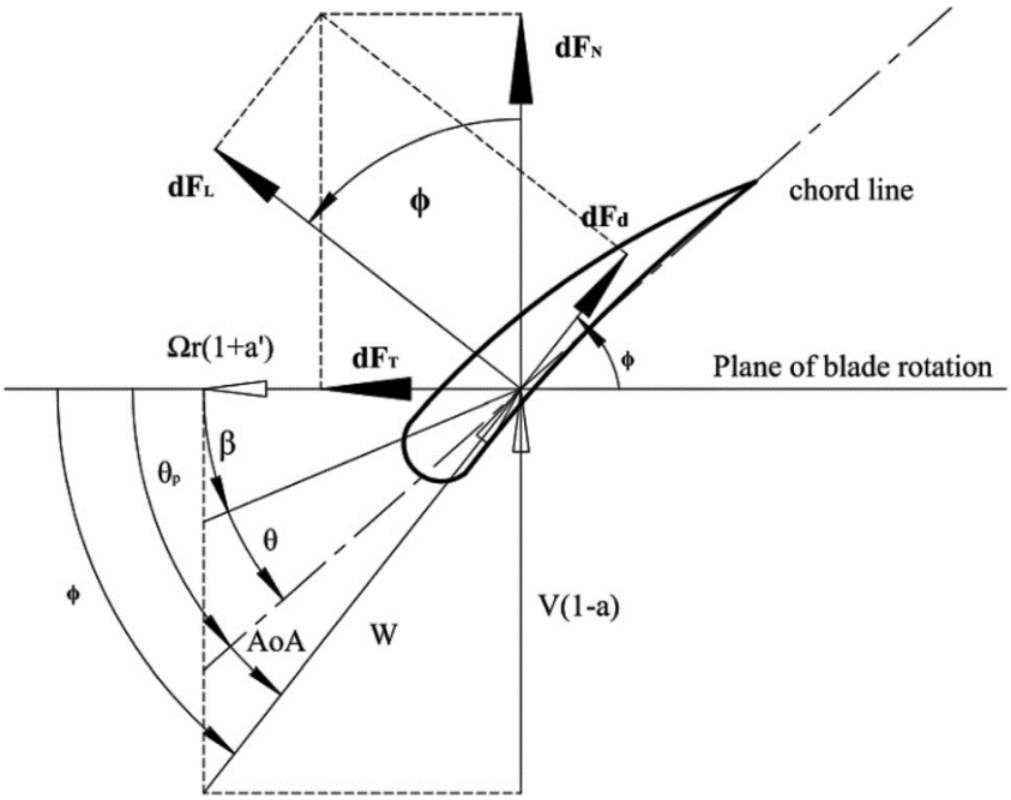

Figure 3.12 Blade section of a horizontal axis wind turbine
(Source: Hu and Rao 2011)

The methodology created for this study and the intermediate steps created by manual calculations are explained in Figure 3.13. It is important how the section pitch angle is determined here. For this reason, it is necessary to explain how to position it to get maximum efficiency from the selected airfoil.

In order to calculate the Reynolds number, it is necessary to find relative velocity(W) by initially assuming axial(a) and tangential(a') induction factors zero. This will allow us to easily calculate the relative velocity and inflow angle(ϕ).

The airfoil lift coefficient vs. angle of attack graph is obtained using the XFoil software for the Reynolds number calculated. The angle of attack(AoA) which airfoil has the maximum lift coefficient is accepted as a section angle of attack.

In order for the angle of attack(AoA) to be at the desired value, the section pitch angle(θ_p) is obtained by subtracting the angle of attack(AoA) from the calculated inflow angle(ϕ) and the airfoil is positioned accordingly.

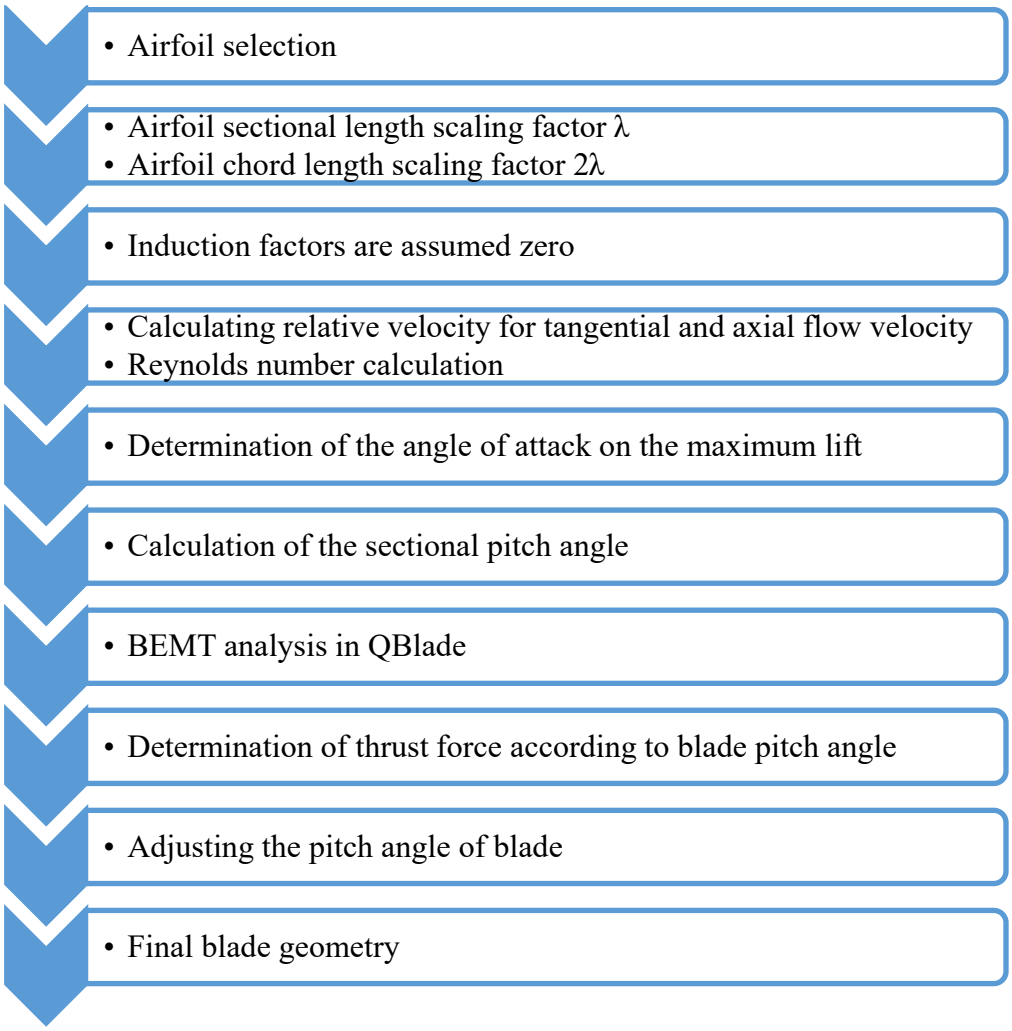

Figure 3.13 Steps for modelling methodology

Choosing the airfoil to be used in the design is the most important factor affecting the performance. Looking at the desired working conditions and the dimensions of the blade, it is observed that blade is operated at low-Reynolds number speeds between 7,000 to 25,000. For this reason, it is necessary to choose an airfoil that perform better at low-Reynolds numbers.

There are two different types of low-Reynolds airfoils used in similar studies, these are AG04 used in study of Martin (2011) and SD7032 used in study of Bayati (2017). These airfoils are selected for use in modelling study and their geometry can be seen in Figure 3.14, 3.15 and 3.16. In addition, Ishii airfoil (Anyoji et al. 2014) designed for the Mars project is also considered.

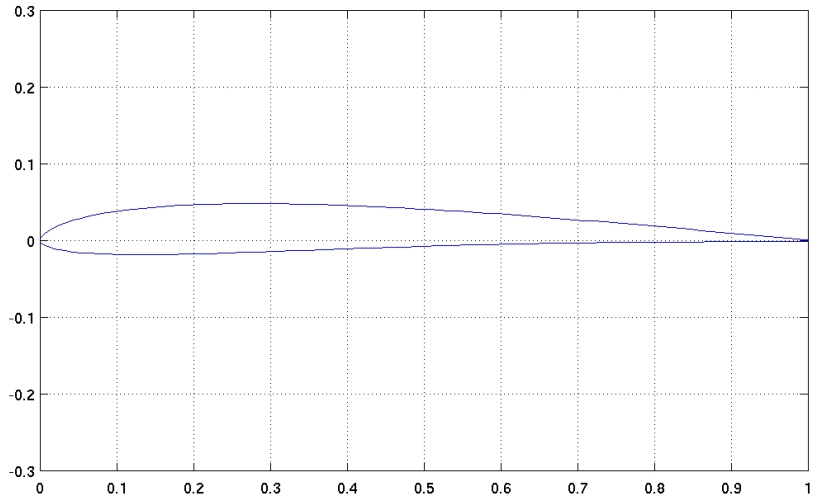

Figure 3.14 AG04 airfoil
(Source: UIUC Applied Aerodynamics Group 2020)

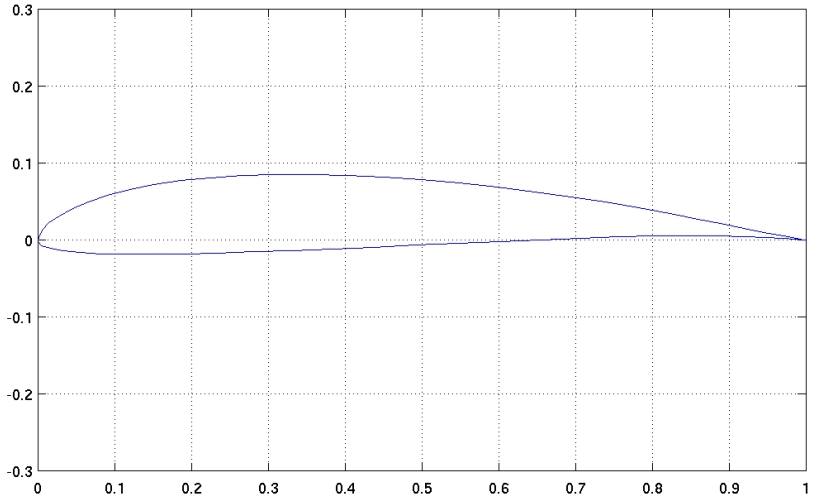

Figure 3.15 SD7032 airfoil
(Source: UIUC Applied Aerodynamics Group 2020)

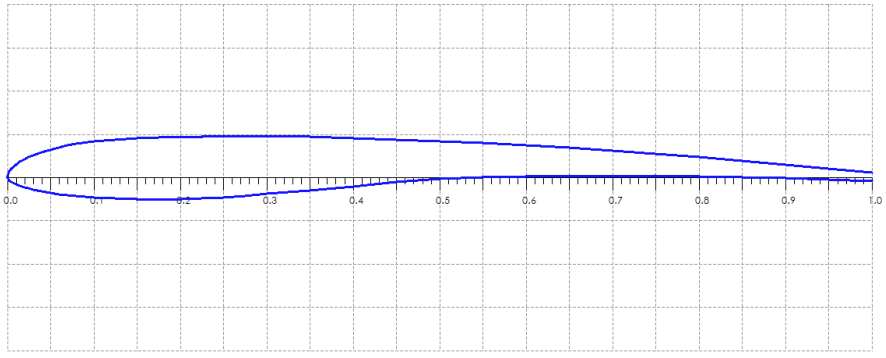

Figure 3.16 Ishii airfoil
(Source: Anyoji et al. 2014)

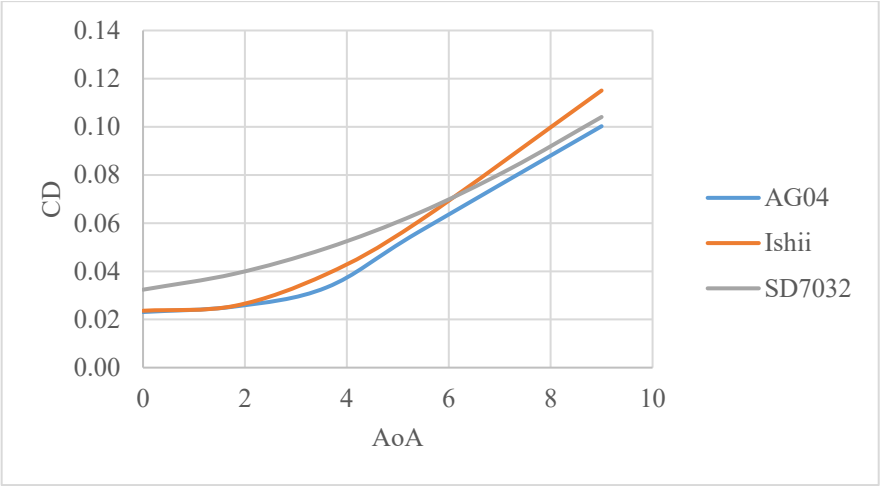

Figure 3.17 Drag coefficients with respect to angle of attack at Re=19200

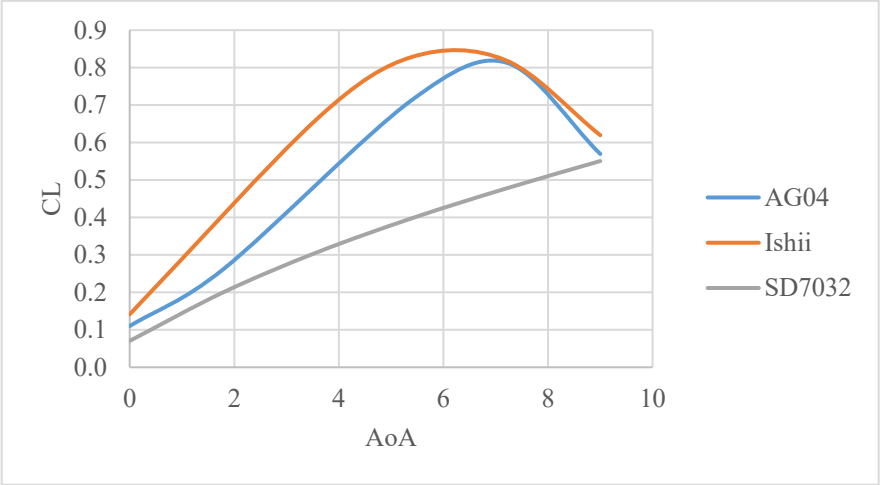

Figure 3.18 Lift coefficients with respect to angle of attack at Re=19200

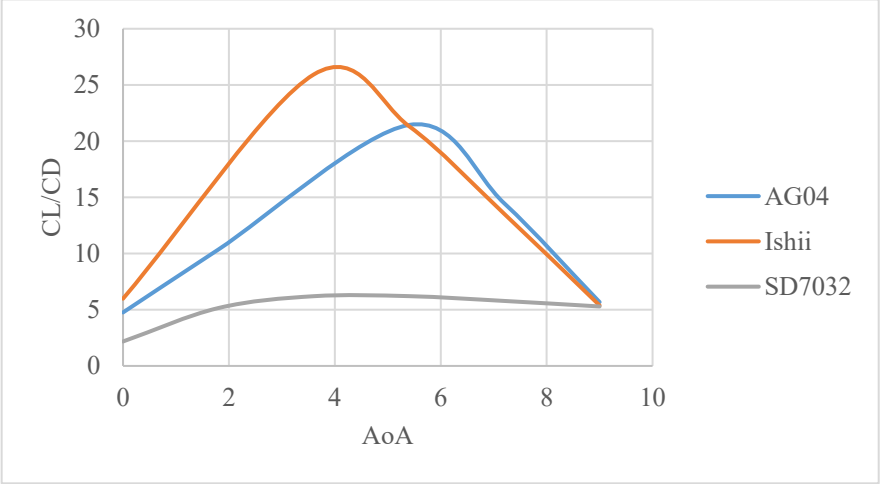

Figure 3.19 Ratio of lift and drag coefficient with respect to angle of attack at Re=19200

It was analyzed using XFoil software to observe the performance differences between the airfoil profiles used in the model design. The analyzes were made at the Reynolds number of 19200 which is the average Reynolds number of the model wind turbine. The drag coefficients of the airfoils are very close to each other, as seen in Figure 3.17. It is observed that Ishii airfoil produces more lifts than others in Figure 3.18. The ratio of lift coefficient to drag coefficient is the best graph where airfoil profile performance can be observed in Figure 3.19. As can be seen here, the performance of Ishii airfoil is better than the other two airfoils.

Modelling calculations were made with three different blades each made by one of these three airfoils under the conditions of 3.16 m/s wind speed, 316.22 rpm and 4.71 TSR. The results of rotor analysis are given in the Table 3.4. The results show that all the blades give very small power coefficient. Two of them even gave negative power coefficients which means that those blades require extra power from outside to reach that rotational speeds. The study with Ishii airfoil is the only one that give a small positive power coefficient. As long as the thrust coefficients are concern, all of the blades perform very similarly. Therefore, among these three airfoils, Ishii is chosen due to its positive power behavior.

Table 3.4 BEMT result of model rotors

Airfoil of Blade	Power (W)	Power Coefficient	Thrust (N)	Thrust Coefficient
AG04	-0.148	-0.0120	0.302	0.0776
Ishii	0.138	0.0112	0.303	0.0778
SD7032	-0.144	-0.0117	0.298	0.0765

In order to validate the rotor results obtained by the analysis of the blade formed with Ishii airfoil with QBlade, it was compared with a CFD analysis done by Dr.Sercan Acarer. The power and thrust values obtained by CFD analysis are 0.39 W and 0.32 N, respectively. The volume and solution methods used for CFD analysis are given in Appendix D.

Geometrical data of the blade created with Ishii airfoil are given in the Table 3.5 and its cross sections are shown in the Figure 3.20. Thread axis data refers to the point where the y axis passes in Figure 3.20.

Table 3.5 Geometrical data of model blade

Section	Airfoil	Radial Position (m)	Chord Length (m)	Twist Angle (Degree)	Thread Axis (%Chord)
1	Cylinder	0.05000	0.03000	37.5400	0.500
2	Cylinder	0.08000	0.03000	35.3900	0.500
3	Ishii	0.11000	0.08000	37.5412	0.222
4	Ishii	0.13548	0.07310	33.2434	0.222
5	Ishii	0.16093	0.06687	29.5453	0.222
6	Ishii	0.18640	0.06116	26.5468	0.222
7	Ishii	0.21187	0.05591	23.7482	0.222
8	Ishii	0.23734	0.05115	21.3495	0.222
9	Ishii	0.26281	0.04675	19.6503	0.222
10	Ishii	0.28828	0.04250	18.6508	0.222
11	Ishii	0.31374	0.03864	17.3515	0.222
12	Ishii	0.33921	0.03513	16.2520	0.222
13	Ishii	0.36468	0.03193	15.2525	0.222
14	Ishii	0.39015	0.02903	14.2531	0.222
15	Ishii	0.41562	0.02639	13.4535	0.222
16	Ishii	0.44108	0.02613	12.8538	0.222
17	Ishii	0.44553	0.02500	12.6539	0.222
18	Ishii	0.44775	0.02000	12.6539	0.222
19	Ishii	0.44887	0.01500	12.5539	0.222
20	Ishii	0.44944	0.01000	12.5539	0.222
21	Ishii	0.44972	0.00750	12.5539	0.222
22	Ishii	0.45000	0.00005	12.5539	0.222

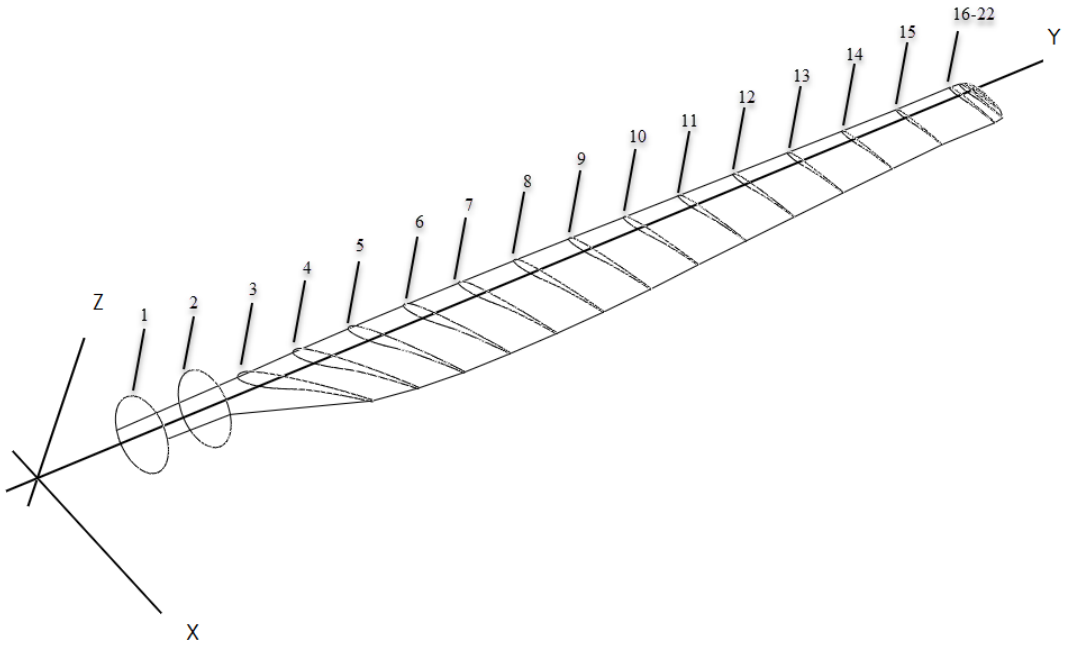

Figure 3.20 Model blade illustriation

3.4. Design of Model Wind Turbine

In this study, model turbine design is done by assuming that the tower and the blades behave like a rigid body without any flexibility. The mass distribution of the model turbine is created very similar to the reference turbine according to the scaling method. Table 3.6 gives the mass data of the parts used in the design.

Table 3.6 Mass properties of wind turbine

Parameters	Reference	Scaling Factor	Desired Model
3 blade mass	5322 kg	λ^3	83.15 gr
Tower mass	34900.7 kg	λ^3	545.32 gr
Nacelle mass	21796 kg	λ^3	340.56 gr
Hub mass	4420 kg	λ^3	69.06 gr
Total mass	66438.7 kg	λ^3	1038.10 gr

Creation of the entire blade relies on the geometric data of the blade sections given in Table 3.5. The blade is constructed by the loft feature of the mechanical design software, Solidworks 2018. In the Solidworks software, a groove for the hub connection is made at the root of the blade and prepared for the hub connection, final blade geometry is shown in Figure A.3, and the resulting blade volume is calculated as 67150 mm^3.

The model blade is the most difficult part to produce in this design because of its complex geometry which includes may thin cross sections and twisted surfaces. There are three methods considered as production; these are i- plastic injection which requires a mold although an expansive mold production, ii- carbon fiber production which also requires a mold although less expansive and a very qualified workmanship and finally iii- 3d printing which is the most flexible and least expansive method. It has been observed that it is very difficult to produce the mold in plastic injection and carbon fiber methods because the blade thickness goes below 1mm in some regions. Another issue is to produce a very light blade which requires to produce a hollow blade with a very thin shell so that the desired mass can be obtained. This is not possible with the first two methods.

Some tryouts were made with the only option, the 3d printing method. ABS, Nylon-Carbonfiber and STH were used as filaments in the 3d printer. Excessive surface

deterioration was observed in the blade produced using ABS (Figure 3.21). Nylon-Carbonfiber filament was broken from many parts during printing (Figure 3.22). Therefore, printing was abandoned with these two filaments. With the STH filament (Figure 3.23), an almost smooth surface was obtained by adjusting the fill rate and was not broken in the manual strength test. In the STH, which was chosen as the lowest mass and best strength, 36 gr blade mass was obtained.

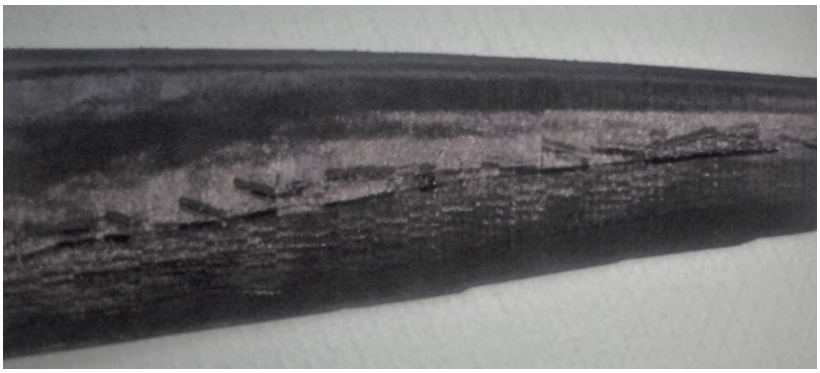

Figure 3.21 ABS printed blade

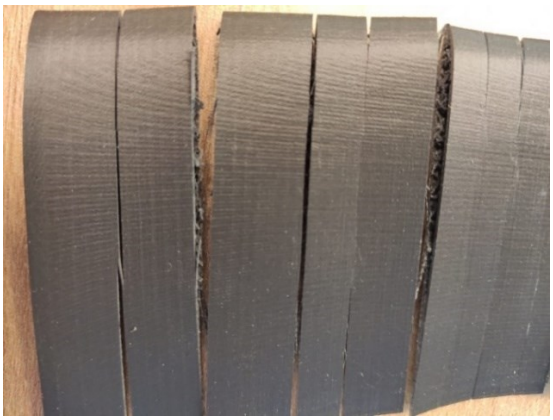

Figure 3.22 Nylon-Carbonfiber printed blade

Figure 3.23 STH printed blade

The tower geometry of the reference turbine has a constant diameter from the root to the middle of the tower and a geometry with a decreasing diameter from the middle of the tower to the tip. For tower modeling, the reference tower consisting of 36 meters in length and various diameters is averaged to a fixed diameter by calculating the weighted average diameter of 2.05 m. The drag coefficient of the prototype tower at a speed of 20 m/s is found as 0.8. In order to make a correct modeling, the drag coefficient of the model and the reference tower must be the same. Since the model Reynolds number is found as 2x10^3 (wind speed of 3.16 m/s), the drag coefficient is about 1.0 and it cannot be made the same as prototype. In other words, if the tower is just scaled down according to geometrical scaling factor, the drag force would be 20% higher than what it is supposed to be. Therefore, in order to keep the drag force on the tower at the desired level, smaller diameter must be used. This strategy leaded for a model tower diameter of 20 mm instead of 51.25 mm.

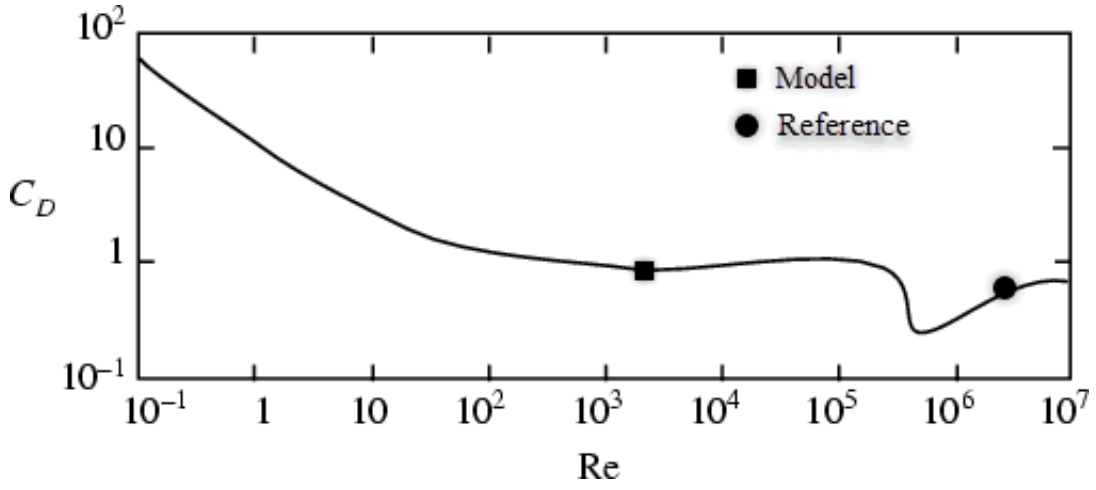

Figure 3.24 Average drag coefficient for crossflow over a smooth circular cylinder (Source: Schlichting and Gersten 2016)

The hub diameter of the model is calculated as 0.05 meters according to the reference turbine with a hub diameter of 2 meters by using scaling methodology. The nacelle part positioned on the top of the tower is designed as small as possible compared to the diameter of the hub and it is provided to be less affected by the drag force that will occur.

The nacelle and tower link are designed as a rail mechanism and fixed by a setscrew. The reason for this is to solve the small center of mass errors that will arise from production and assembly by shifting along the tower and nacelle axis, see in Figure 3.21.

According to the scaling methodology, it is necessary to capture the tip speed ratio in order to achieve dynamic similarity on the aerodynamic part as close as possible. It is seen by BEMT analysis that it is impossible for the model turbine to reach 316.22 rpm at 3.16 m/s wind speed by itself (very low power coefficient), so the rotor must be driven by a motor attached to the nacelle to accommodate the required tip speed ratio. Since a turbine tower will be positioned on a floating platform, the loads coming to the rotor can change due to the platform movements and the motor should turn at constant speed with changing loads. It is important to choose an appropriate motor and a driver that can meet these conditions. For this reason, the motor and driver that can be used with PID support given in Table A.1 were found suitable for this study. In addition, since the weight of the motor to be chosen is also important, the 98gr motor given in the table is preferred.

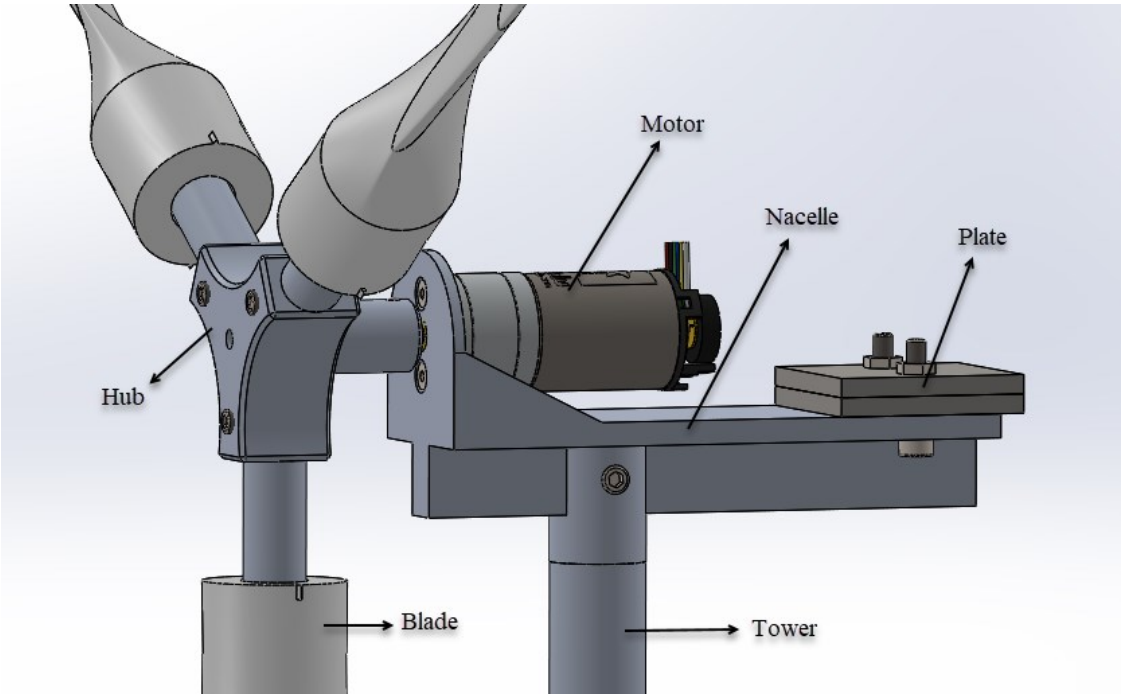

Figure 3.25 Model wind turbine design drawing

Matching the center of gravity of the reference turbine is very important for the dynamic response of the model. The center of gravity of the reference wind turbine is

found to be located on the tower axis and 26.24 meters above the ground. According to scaling the center of gravity in the model turbine have to be 0.65 meters above the ground. With the parts designed as small and light as possible and using 6000 series aluminum to be light in weight, the center of mass is found at the front of the turbine. In order to pull the center of gravity to the tower axis, weight plates designed from 304 steel are placed on the back of the nacelle, as seen in the Figure 3.25.

Mass distribution information is given in Table 3.7, technical drawings of the model turbine are included in Appendix A.

Table 3.7 Mass distribution of model wind turbine

Turbine Parts	Desired mass	Model Parts	Model cad mass
3 blades	85.15 gr	3 blades	110.88 gr
Tower	545.32 gr	Hub-tower connector Tower-upper part Tower-bottom part	495.80 gr
Nacelle	340.56 gr	Nacelle Motor Plates	322.81 gr
Hub	69.06 gr	Hub Blade-hub connectors	105.47 gr
TOTAL	1038.10 gr		1034.96 gr

Each turbine part is designed to have the desired mass feature separately, but as can be seen in Table 3.7, the desired mass for each part is not exactly achieved. The maximum difference between the desired and achieved masses is occurred at the hub and is 52.7%. This is not crucial for this study because it is stated that the turbine will be modeled with a rigid body approach. As seen in the table, the total mass is almost exactly captured and center of gravity is adjusted to the same level as the reference.

CHAPTER 4

EXPERIMENTAL DESIGN

In experimental studies, it is essential to create environmental conditions using scaling methodology. In this study, a wave maker and wind nozzle are designed for the wave flume in the IZTECH civil engineering hydromechanics laboratory to create scaled environmental conditions experimentally. In this chapter, wave maker and wind nozzle designed by Dr. Ünver Özkol and Dr. Bergüzar Özbahçeci (Drafted by Dr. Timuçin Eriş) will be mentioned. Then the traverse mechanism to be used in wind measurement, the mechanism to be used for thrust measurement of the model turbine and the video processing method used to observe the turbine oscillation are also presented.

4.1. Wave Maker

The waves in nature are not regular and the waves to be produced for extreme conditions are also irregular. For this reason, a wave maker which can achieve irregular waves is designed to simulate natural waves in the laboratory. Looking at the literature, there are 3 types of wave generators are seen in the practice; i- Flap paddle, ii- Piston paddle, iii- hybrid.

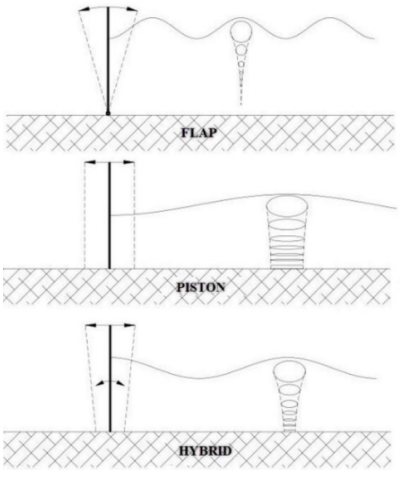

Figure 4.1 Types of wave makers
(Source: Edinburg Design 2016)

When choosing between these three wave generators, the best method for this study in terms of laboratory conditions and desired profile of wave current is the piston type wave maker. The working principle of the piston type wave generator is visualized in Figure 4.1. The wave maker produces waves with the linear motion of the plate placed inside the wave flume and the plate connected to the ball screw, driven by an Ac servo motor. The plate that can move along the wave flume has a 1000 mm stroke.

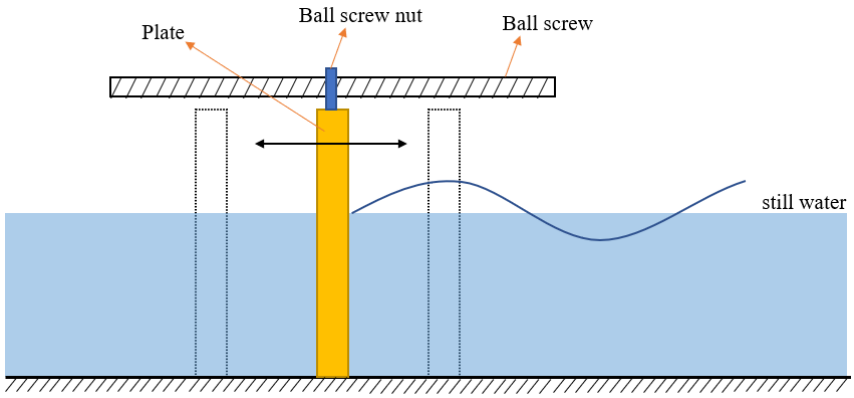

Figure 4.2 Illiillustration of wave maker

The wave maker placed at the beginning of the approximately 40-meter wave flume in the hydromechanics laboratory is shown in figure 4.2. In addition, in order to prevent the generated waves from being reflected by hitting the start/end of the channel, wave-dampening permeable materials were placed in this area.

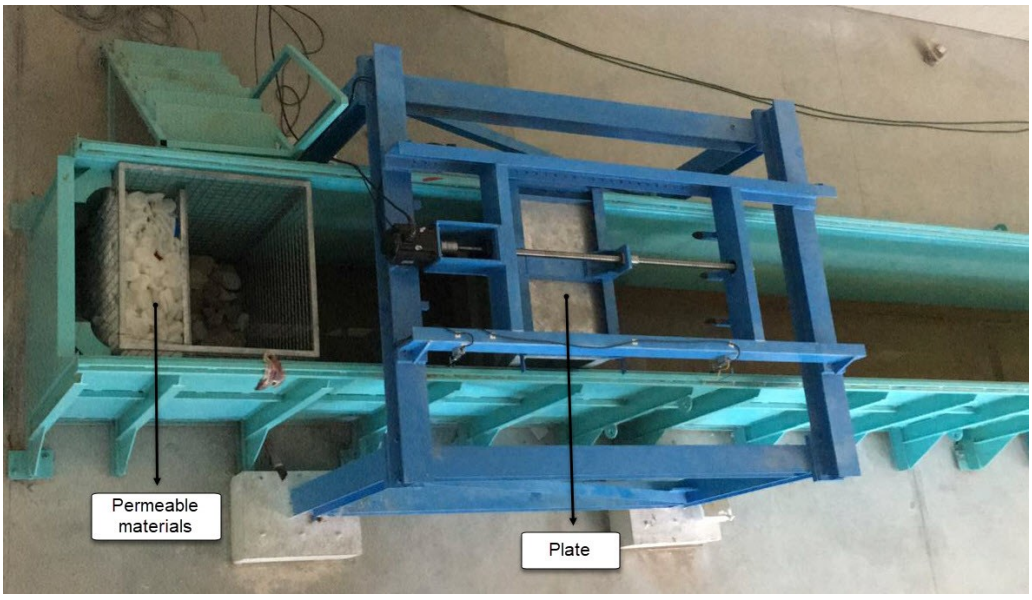

Figure 4.3 Wave maker at the beginning of the wave flume

To prevent wave reflections at the end of the flume after the wave maker, a wave breaking beach with a slope of 1/5 made by stones is constructed which provides a wave damping. The placed stones are shown in Figure 4.4.

Figure 4.4 A wave breaking beach with 1/5 slope made by stones are placed at the endof the tunnel

4.2. Wind Nozzle

Wind profiles in nature are not uniform, so it is necessary to obtain a wind profile like an atmospheric boundary layer profile in experimental studies. For this reason, a wind nozzle is designed in order to create wind on the wave by positioning it on the wave flume. Considering the wave flume dimensions, low turbulence level and smooth velocity profiles, a specially shaped wind nozzle is manufactured with a geometry of a contraction region. The nozzle has 4-to-1 contraction ratio and wall curvatures with 4^{th} degree polynomial. The wind nozzle geometry, as it can be seen in Figure 4.5, has an entrance width of 180x180cm and an outlet of 90x90cm and a length of 360cm. In addition, a perforated plate in 1^{st} section and honeycomb in 2^{nd} section are placed at the entrance in order to distribute the flow across the cross section of the wind nozzle uniformly and to straighten the flow. The perforated plate has 1mm thickness, 9mm hole diameter and the distance between hole centers is 12mm. Honeycomb has 15mm thickness, 10mm cell size and 0.2mm wall thickness.

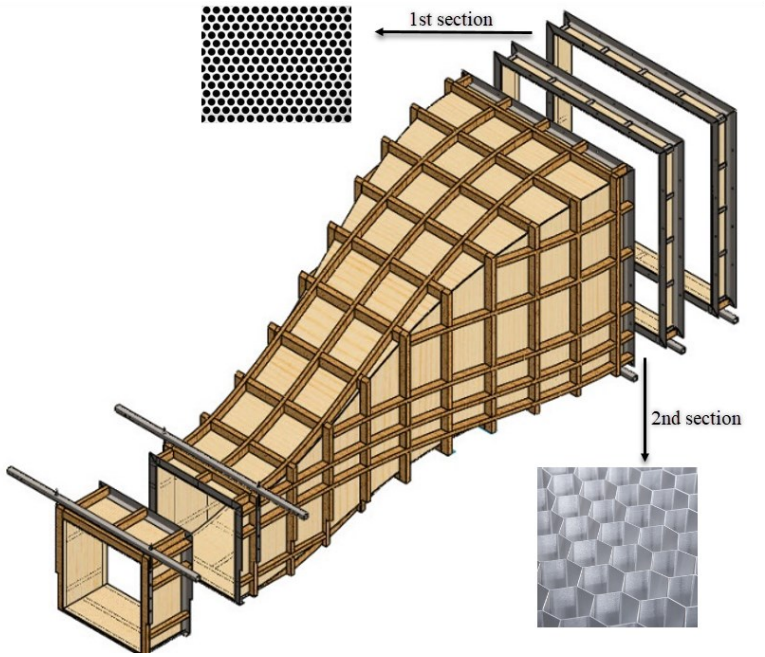

Figure 4.5 Wind nozzle illustration

Four fans, whose speeds can be individually adjusted in order to create gradient and uniform wind profile, are placed in the entrance of the wind nozzle. The wind nozzle placed on top of the wave flume where a part of the nozzle is lowered in to the flume so that a wind profile close to the water surface can be maintained, as seen in Figure 4.6.

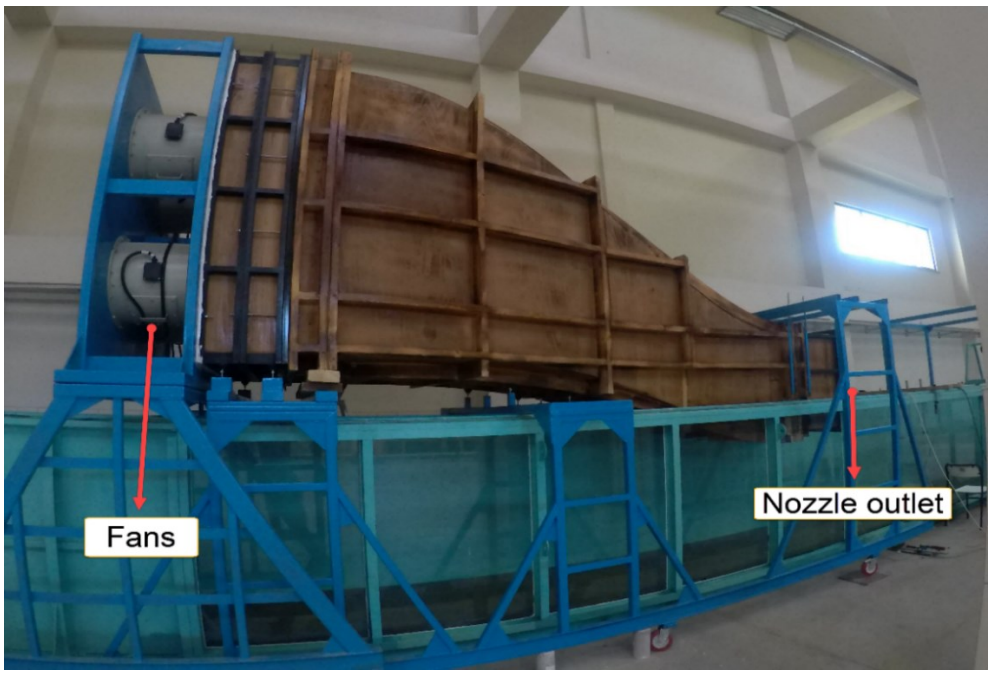

Figure 4.6 Wind nozzle

4.3. Traverse Mechanism for Hotwire Anemometry

Traverse mechanism is needed to position a hotwire sensor in the vertical direction accurately, so that reliable boundary layer profiles can be obtained automatically. The movements along the wave channel direction and wave flume horizontal axis are provided manually in order to reduce the cost in the motion mechanism since high positioning accuracy is not required in those directions. Figure 4.7 shows the traverse mechanism positioned on a carrier.

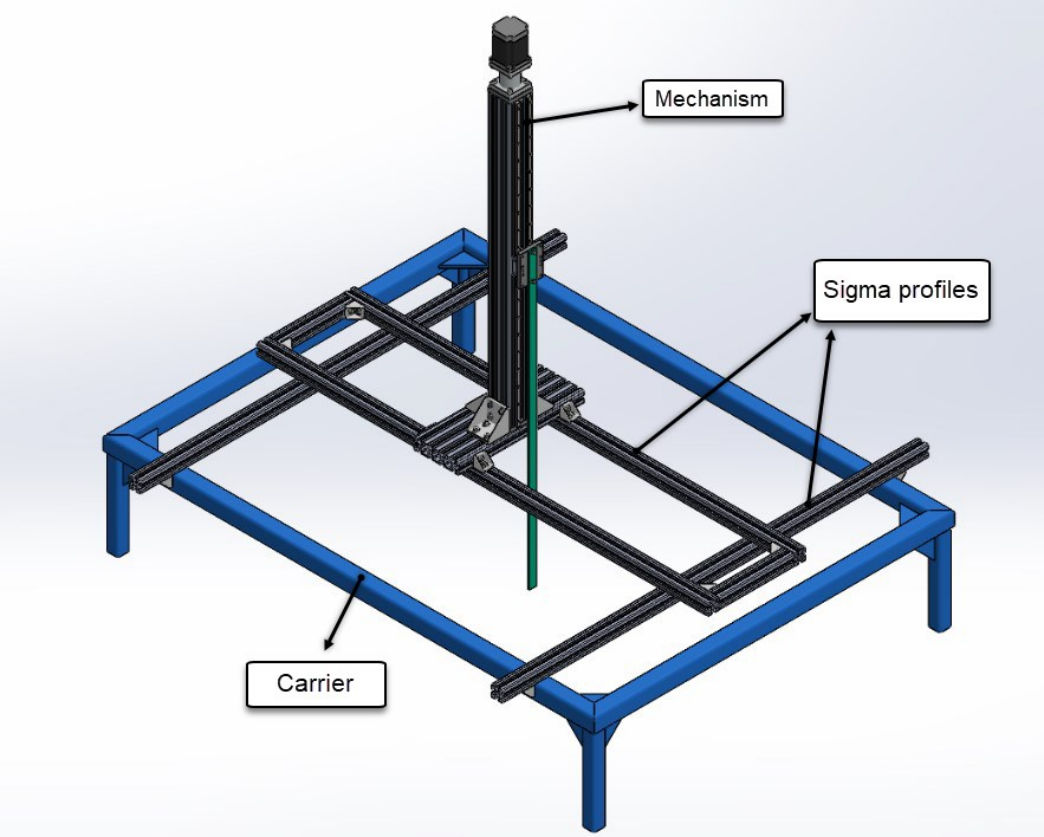

Figure 4.7 Treverse mechanism attached on carrier structure

The mechanism consists of ball screw-nut attached to a stepper motor which has 400 steps per revolution. The ball-nut move linearly on the vertical axis and has a movement precision of 0.1mm. Stepper motor can easily be controlled by a personal computer.

The size of the mechanism is shown in Figure 4.8 (a). Main body is formed with a 90x90mm blank sigma profile, and the cross-section of the mechanism is given in the Figure 4.8 (b).

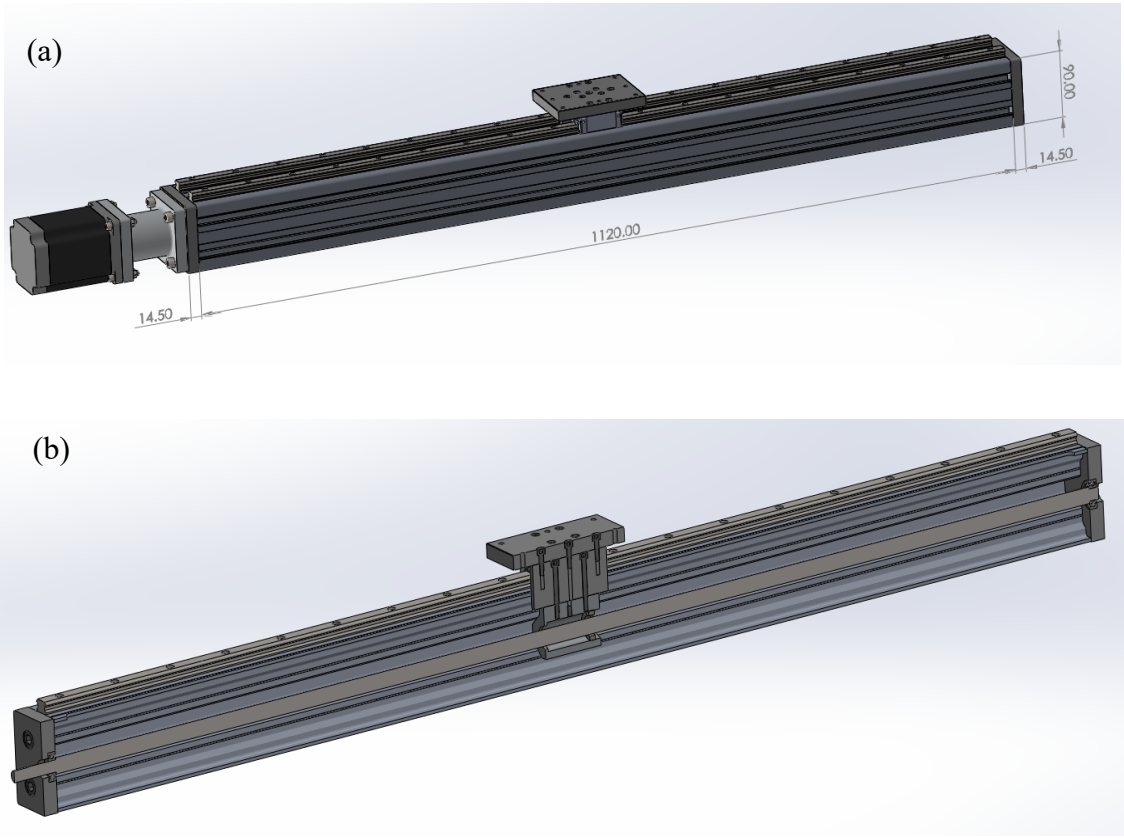

Figure 4.8 Traverse mechanism (a) Dimensions (b) Cross-section

The shaft used in the mechanism has 5mm pitched screw with a 16 mm major thread diameter. The biggest reason for using this shaft is that the backlash ratio is almost zero. Screw is provided with bearings placed at both ends of the shaft, and linear movement along the axis of the rail is provided with cars placed on the precision 15mm wide rails connected to the plate and plates connected to the ball nut. The drive motor used in the system is a step motor with 400 steps, 8.5 Nm torque and holding torque. This stepper motor is driven by a micro step driver to ensure the position accuracy of the mechanism as 0.1mm. A stepper motor, micro step driver and data acquisition card is used to control the mechanism with the computer. To ensure the safety of the mechanism, limit switches are located at the beginning and end of the rails. The electronic equipment used in this system is given in the Table B.1. In addition, the control algorithm of the driver is written using LabVIEW 2014 software and the user interface is created, see in Appendix B.

4.4. Model Turbine Thrust Measurement Mechanism

Thrust measurement mechanism of the model wind turbine is designed to determine the force on the main wind direction. The mechanism resembles a swing mechanism, as seen in Figure 4.10. Turbine tower is placed on a shaft which is free to rotate in the pitch direction. The shaft's rotation is allowed by two ball bearings placed at the both ends. The tower's rotation is balanced by a moment arm which is hold in place by a load cell (the force sensor). The total axial load on the turbine is measured by creating moment on the load cell at a distance of 25 mm from the tower center, technical drawings are given in Appendix C. The total moments acting on the load cell consist of thrust force from the rotor, drag force from the tower and the gravitational force from the turbine mass. With a known wind profile, the drag force acting on the tower can be calculated analytically. Gravitational moment occurs due to the turbine oscillation. The moment created by the center of mass of the turbine over time can be followed and calculated by the video process method. Since total moment can be obtained from the load cell, the thrust force can be obtained by subtracting the other forces from total.

$$M_{Thrust} = M_{Total} - M_{Drag} - M_{Gravitational} \tag{4.1}$$

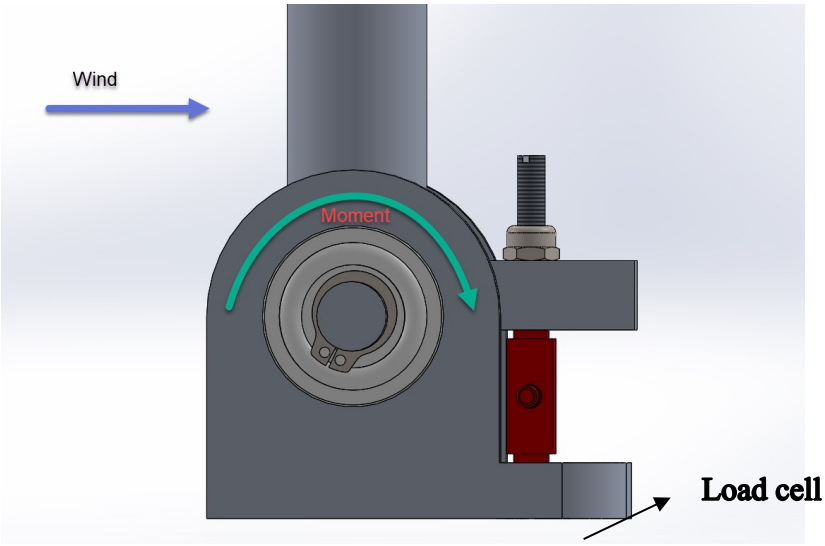

Figure 4.9 Thrust measurement mechanism

The cross-sectional image of the mechanism is also given in Appendix C. Materials of the mechanism are chosen as 6000 series aluminum to provide light weight

and enough strength. The load sensor and amplifier used in this mechanism are given in Table C.1. The total mass of the mechanism with the sensor is 197.54 gr. This mechanism mass is considered as an extra mass in the model platform studies and the model platform is designed accordingly.

As a result of these designs, assembly of model platform and turbine is given in Appendix E with center of gravities.

4.5. Wind Turbine Motion Sensing by a Video Processing

A video processing method is used to observe the oscillation of the model turbine on the model floating platform and it aims to determine its angle change with respect to the ground. This method does not require extra sensors to be placed on the model and does not add extra mass on it. Therefore, it is preferred method in scale model studies.

Tracker (Brown 2009a) is an open source software, which is used in the literature for the purpose of physics education and academically, is preferred. A tracking example and software user interface is shown in Figure 4.10.

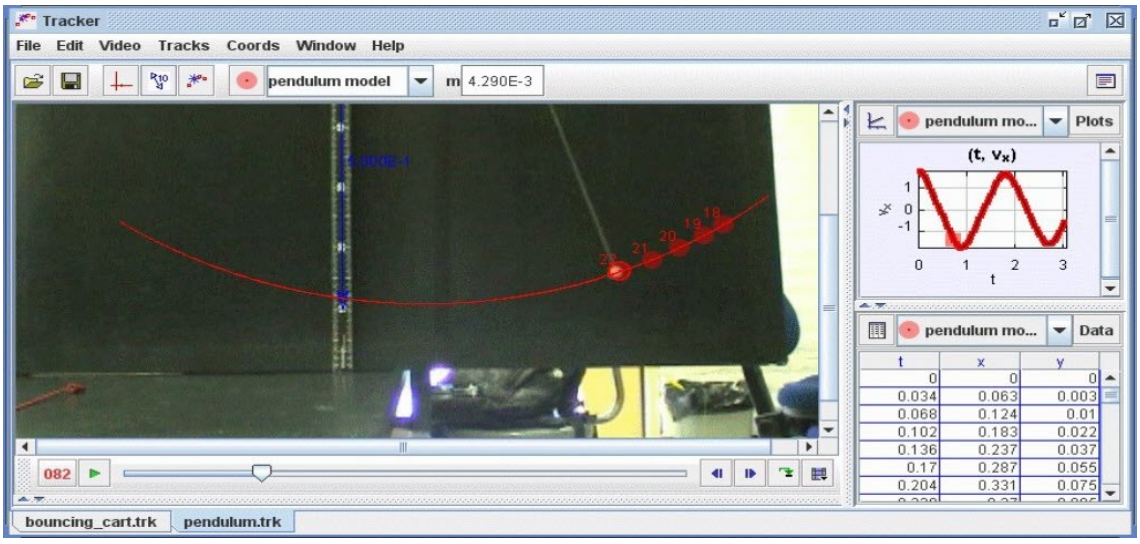

Figure 4.10 Pendulum Example (Source: Brown 2009b)

The operating logic of this software is based on tracking of a defined pixel over color differences. The visual perception system is made according to the recognition of the red-green-blue (RGB) differences. For this reason, the camera recording should be

taken and processed in this software with a marker to be placed in the center of gravity of the turbine. A marker has been designed (Figure 4.11) so that the software can easily identify the pointer and be precise. The marker is drawn according to the frequency order of the RGB colors (Blue> green> red).

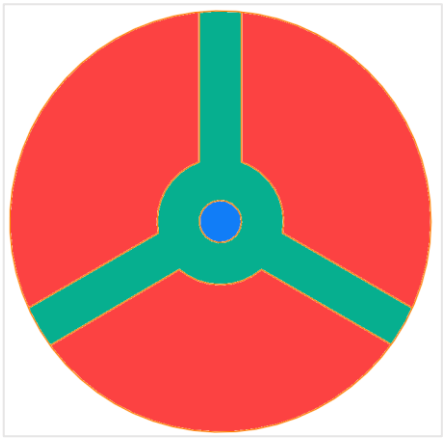

Figure 4.11 Marker

CHAPTER 5

CONCLUSION

The objective of this thesis is to design a model wind turbine to be used as a reference in the experimental studies of a floating wind turbine. This model is expected to have similar dynamical features so that its motions under reference wind and wave loading mimics the prototype floating wind turbine

It was seen that Reynolds number similarity could not be used neither for land based nor for offshore wind turbines due to a very large scaling ratio. With the created scaling methodology, geometric, kinematic and dynamic similarities were achieved only for Froude number and tip speed ratio similitude.

In this study, Blade Element Momentum -BEM- method was used to create a thrust scaled rotor model that can generate some power. Many low-Reynolds number airfoils were tested with this method and only the most promising three different low-Reynolds number airfoils were presented for brevity. As a result of the BEM analysis, blade with Ishii airfoil was observed to generate some power, although very small, and the results were checked by performing CFD analysis. According to the CFD analysis, the power is almost 3 times higher than the BEMT result. In thrust force, 5% difference was observed between CFD and QBlade analysis results. This difference is an acceptable value.

The model turbine, which is modeled using a rigid body approach, was designed according to the scaling methodology which not only satisfies thrust forces but also total mass, mass distribution and therefore satisfies the center of gravity of the model turbine. Similitude of flexibility is not satisfied due to limited resources and time of the project.

Wave maker and wind nozzle are mentioned to create environmental conditions according to the wave flume existing in IZTECH. In order to collect accurate data in the experiments, traverse and thrust measurement mechanisms were designed and video processing method was applied.

In conclusion, a wind turbine has 320kW power was modeled for use in floating wind turbine experiments and that was created as a reference for offshore experimental studies.

APPENDICIES

APPENDIX A

TECHNICAL DRAWINGS OF MODEL WIND TURBINE

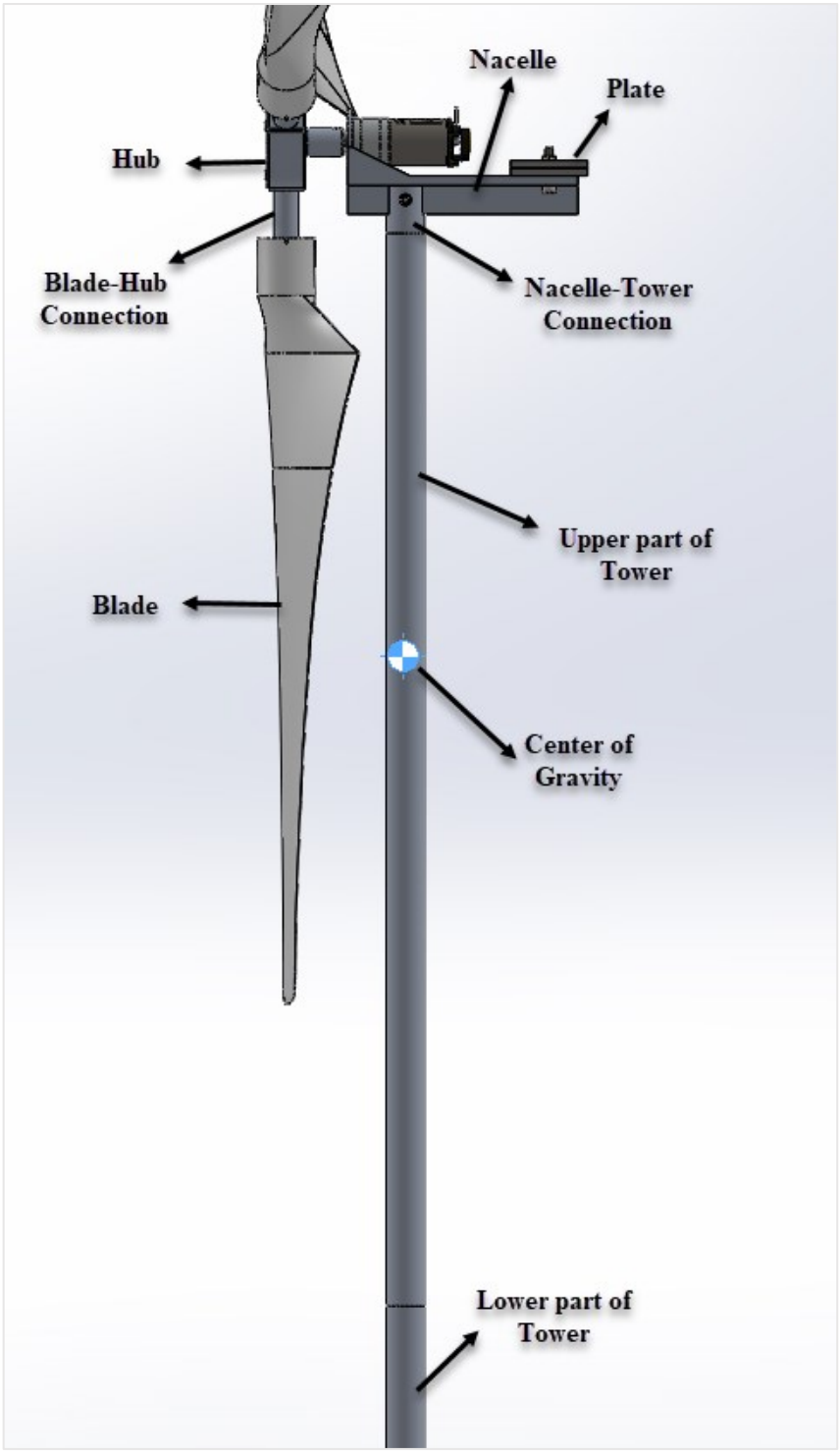

Figure A.1 Parts of model wind turbine

Table A.1 Details of motor and driver

Instrument	Part Number	Part Name
Motor	Pololu #4843	20.4:1 Metal Gearmotor 25Dx65L mm HP 12 with 48 CPR Encoder
Driver	Pololu #3148	Jrk G2 18v27 USB Motor Controller with Feedback

All numerical values are given in millimeters.

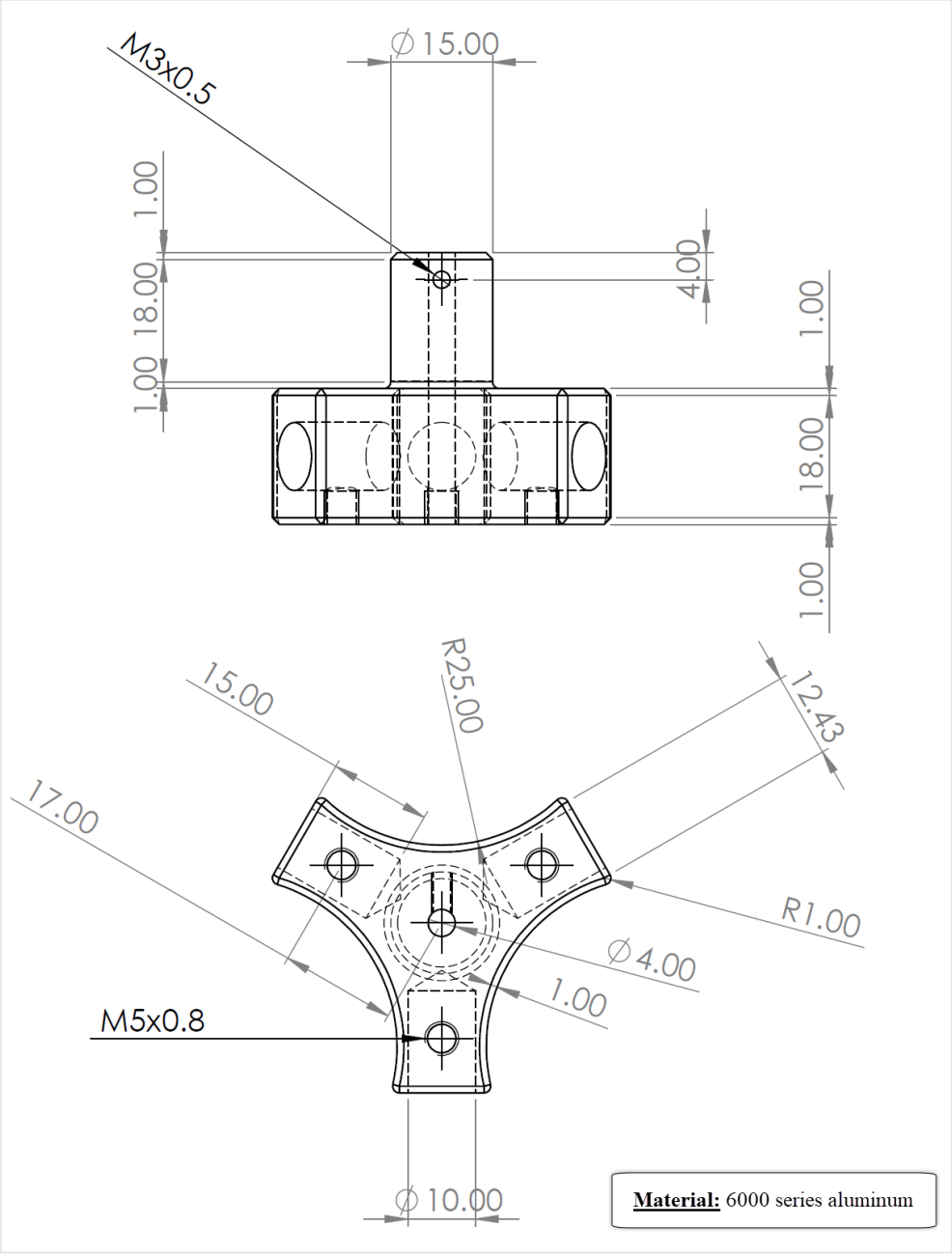

Figure A.2 Hub

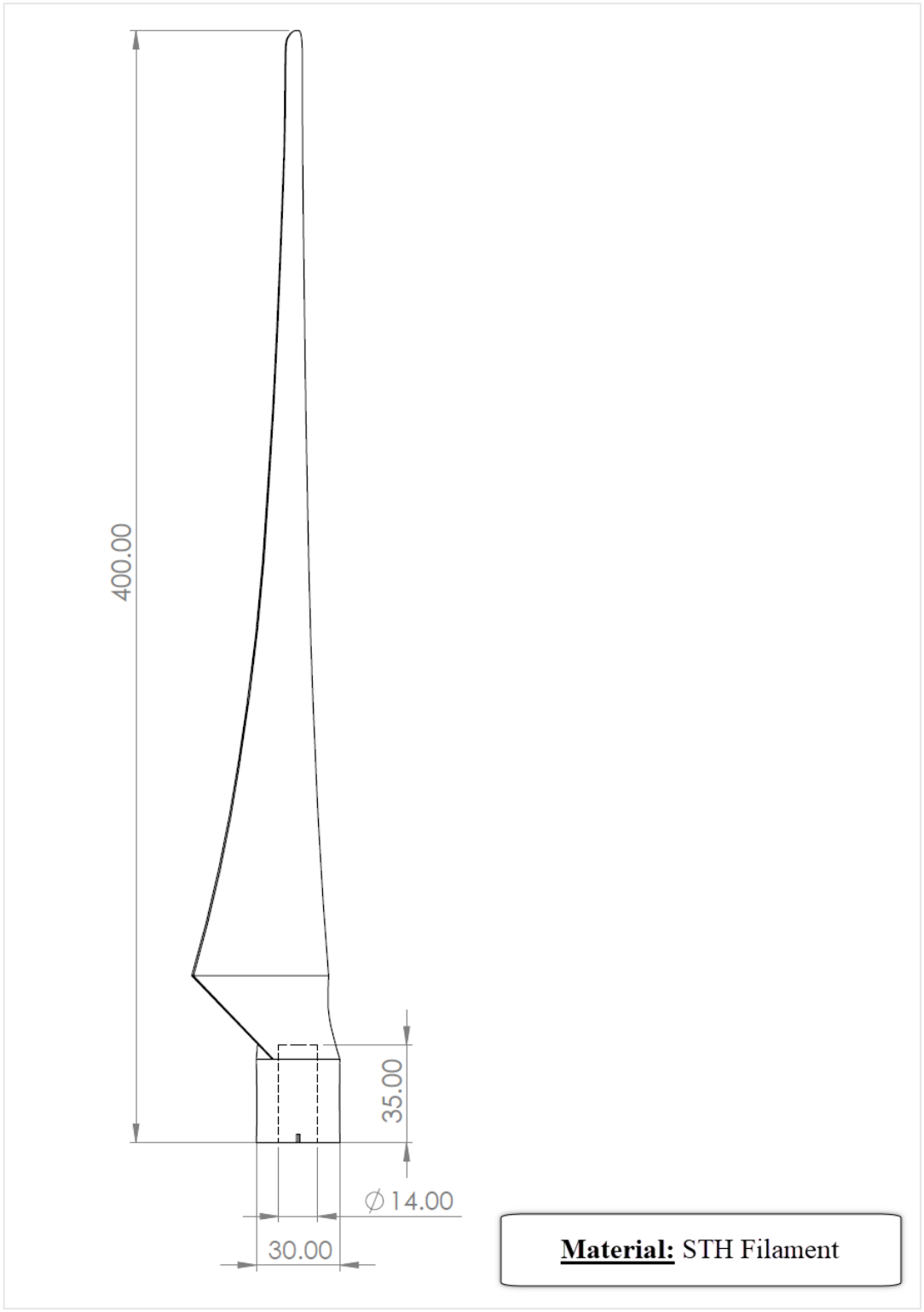

Figure A.3 Blade

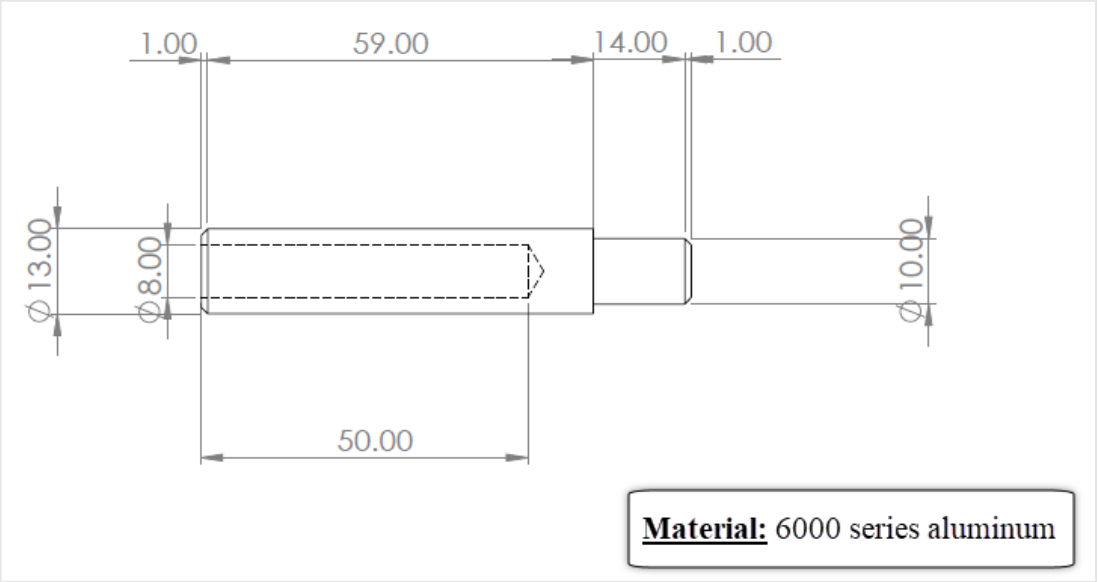

Figure A.4 Blade-hub connector

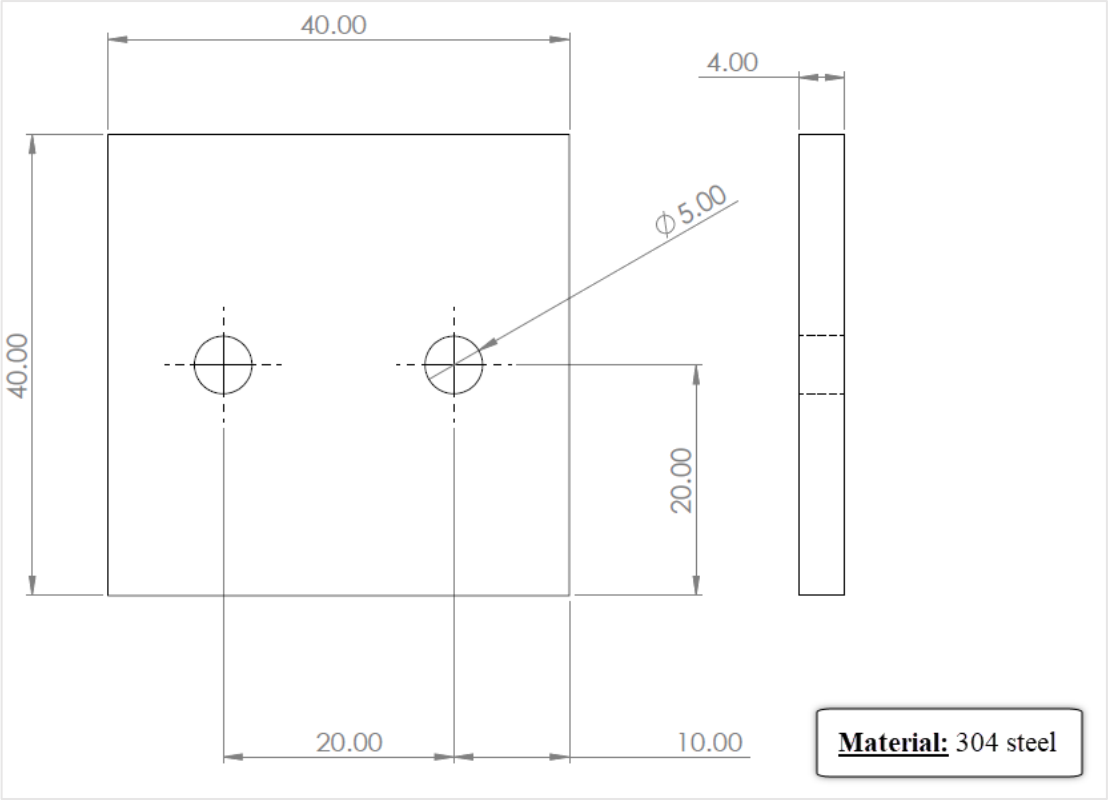

Figure A.5 Plate

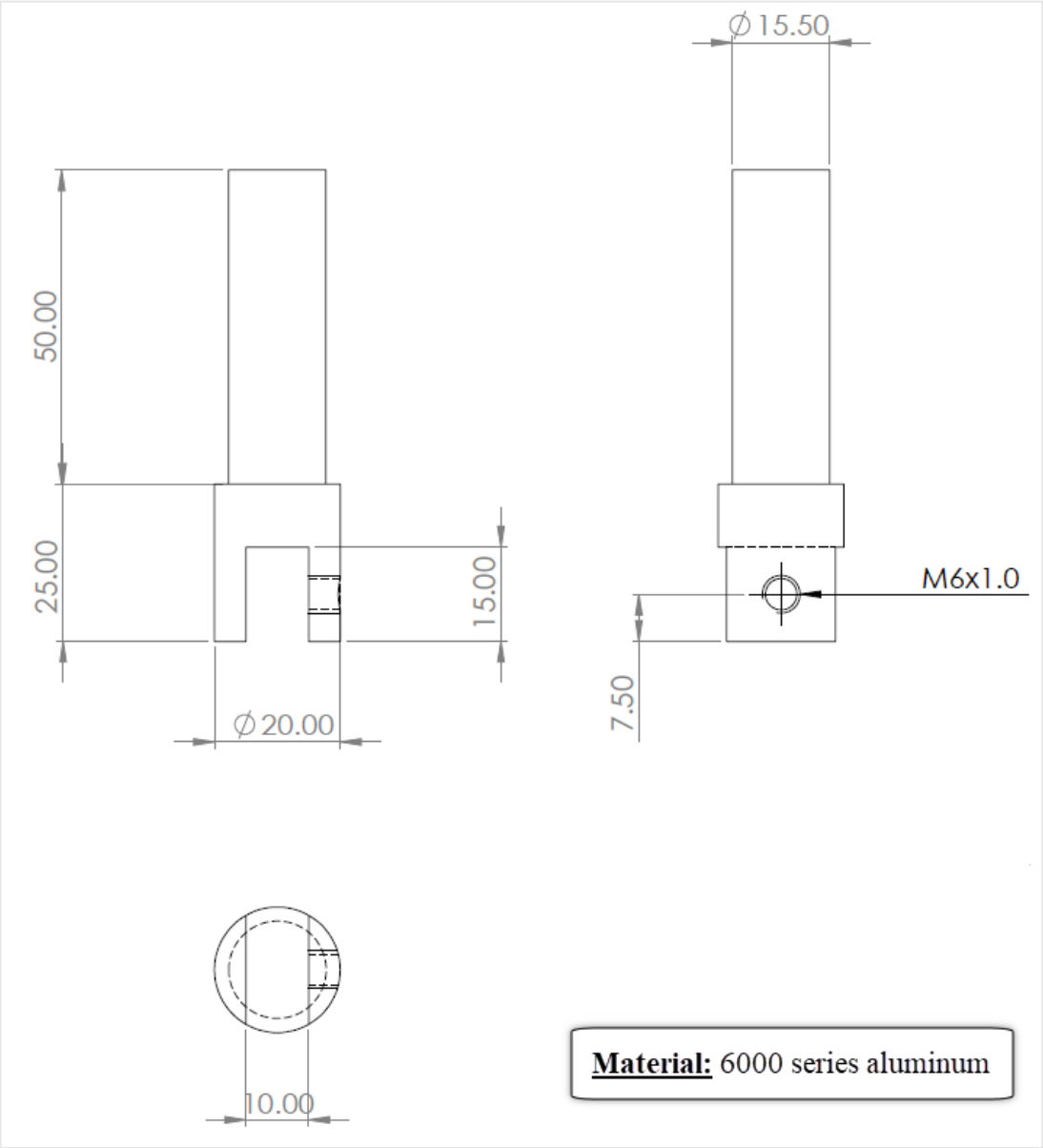

Figure A.6 Tower - nacelle connector

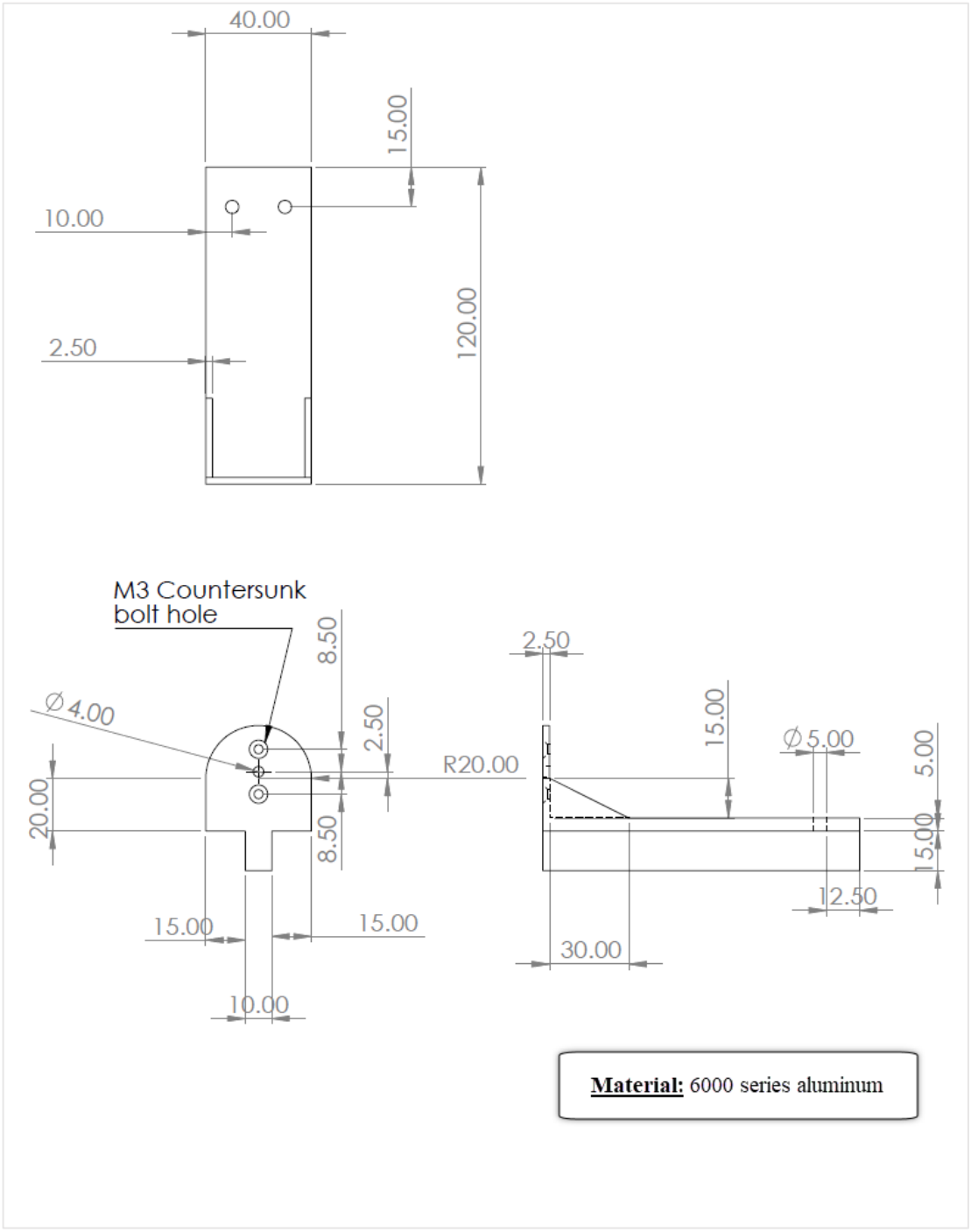

Figure A.7 Nacelle

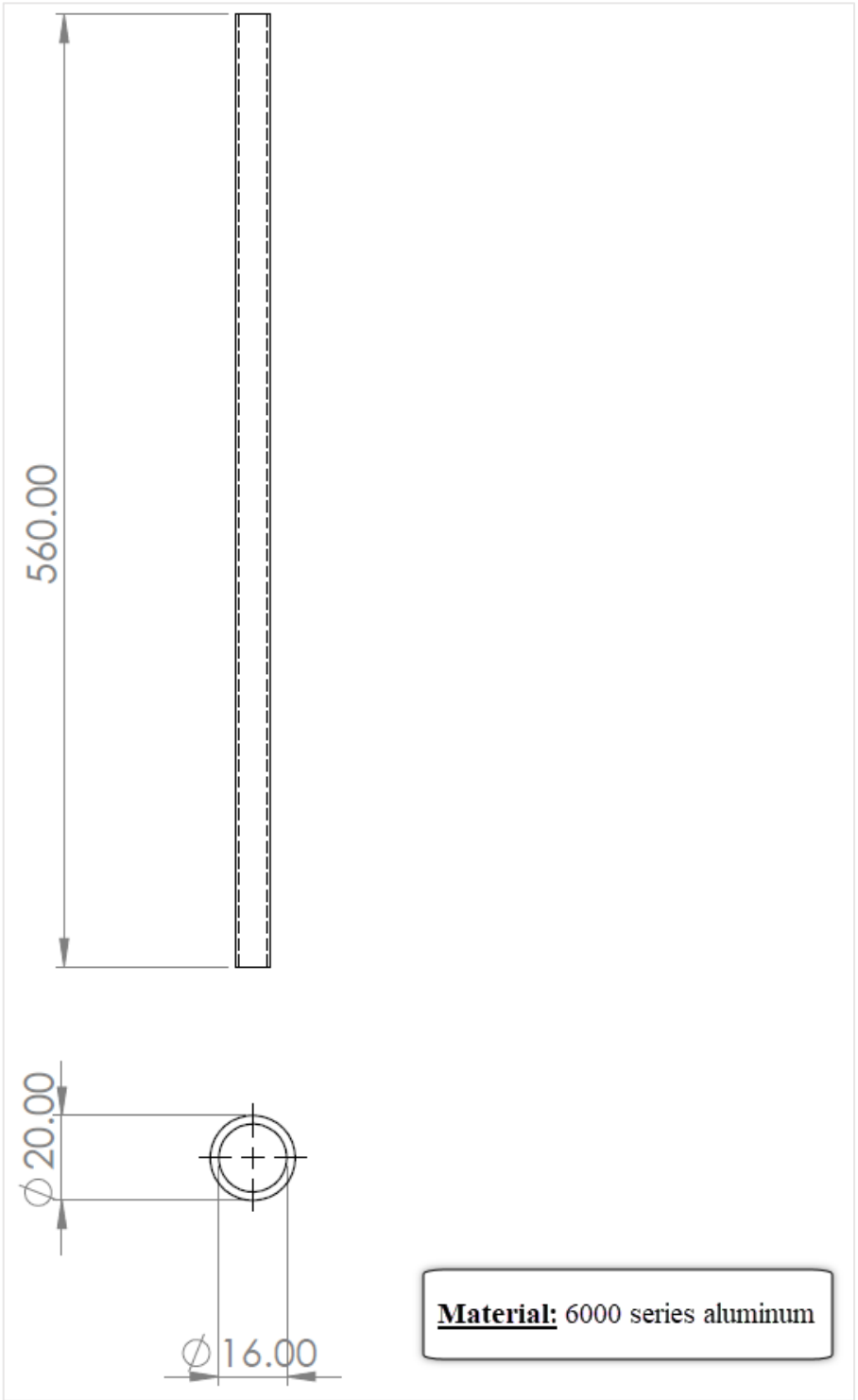

Figure A.8 Tower - upper part

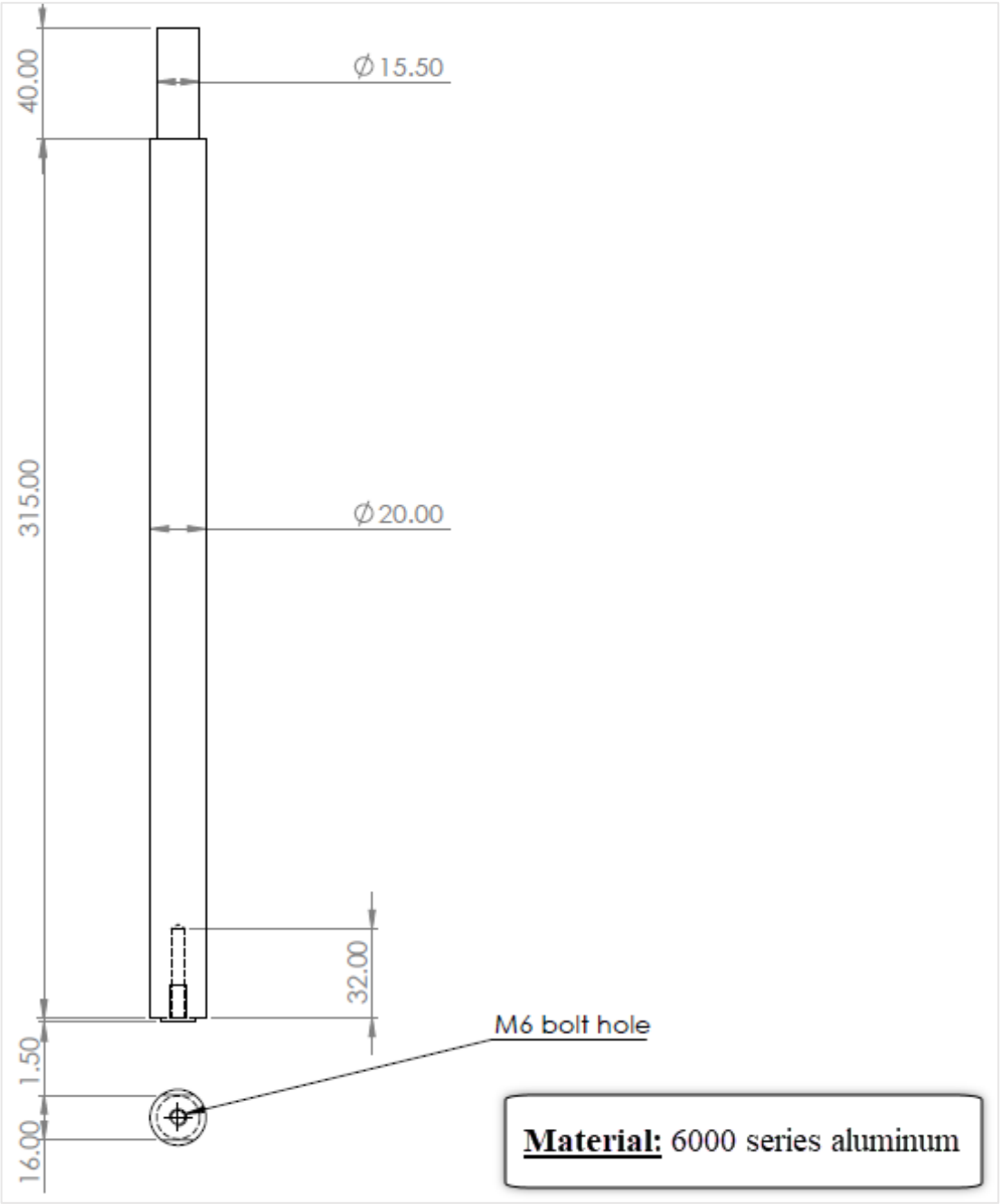

Figure A.9 Tower - bottom part

APPENDIX B

TRAVERSE MECHANISM ALGORITHM

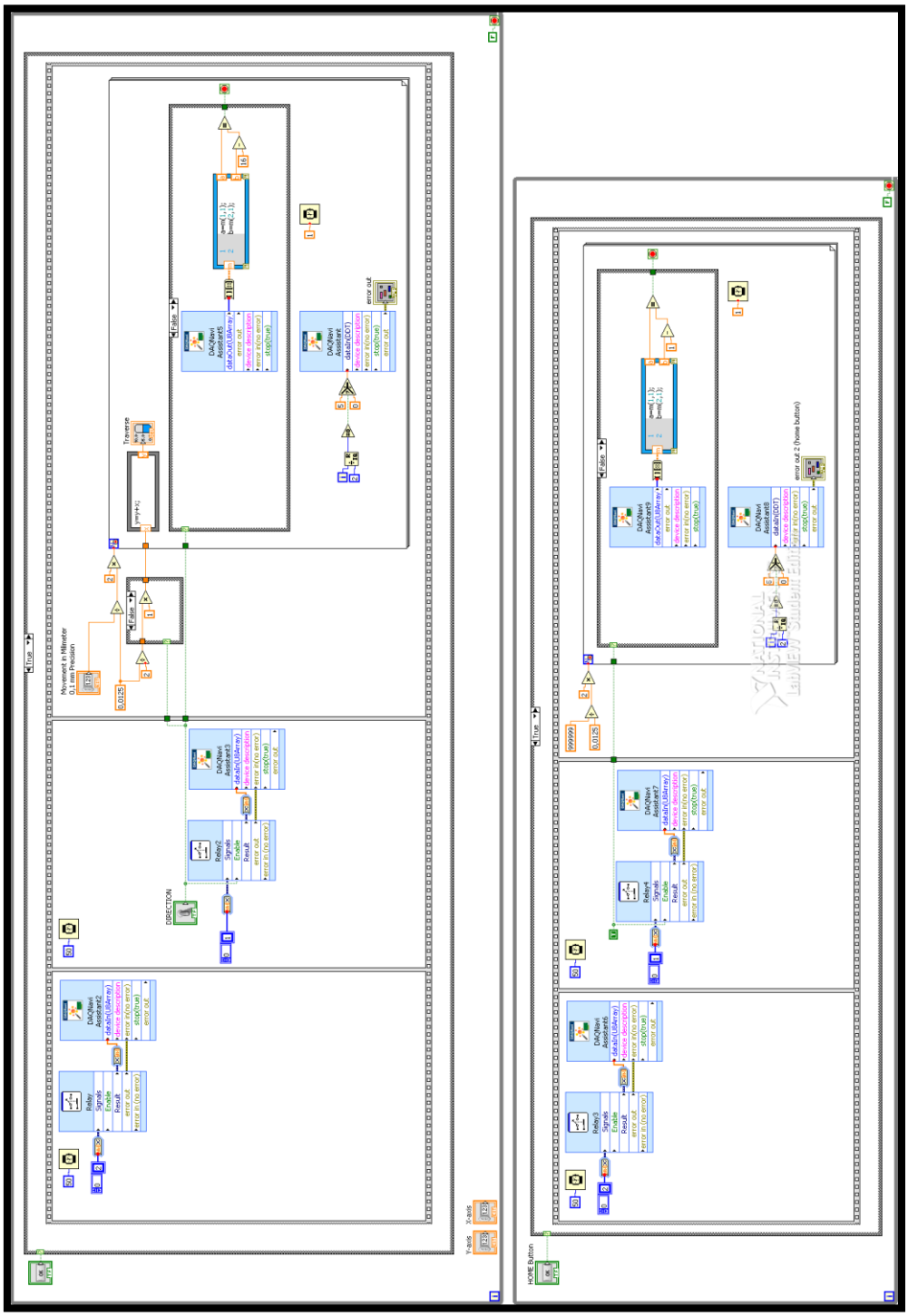

Figure B.1 Mechanism control algorithm

Table B.1 Electronic equipments of traverse mechanism

Part	**Description**
Step motor	Nema 34 8.5Nm
Driver	Leadshine MA860H
Limit switch	Lema LZ15-GW22M-B
DAQ Card	Advantech PCI-1710HG

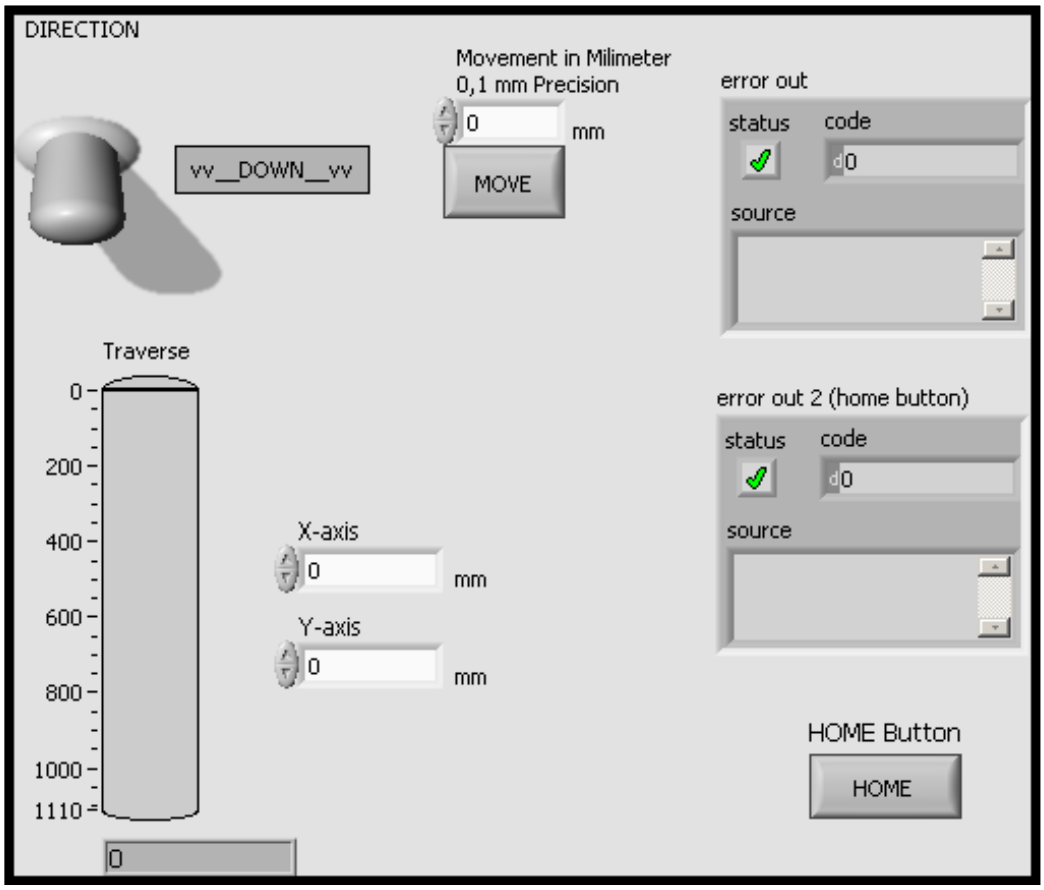

Figure B.2 User interface

APPENDIX C

THRUST MEASUREMENT MECHANISM

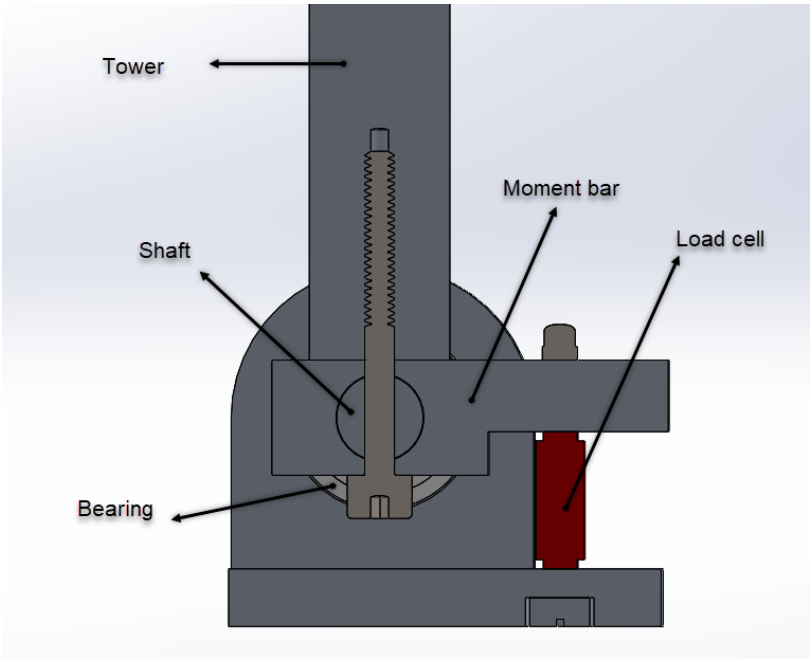

Figure C.1 Cross-section of mechanism

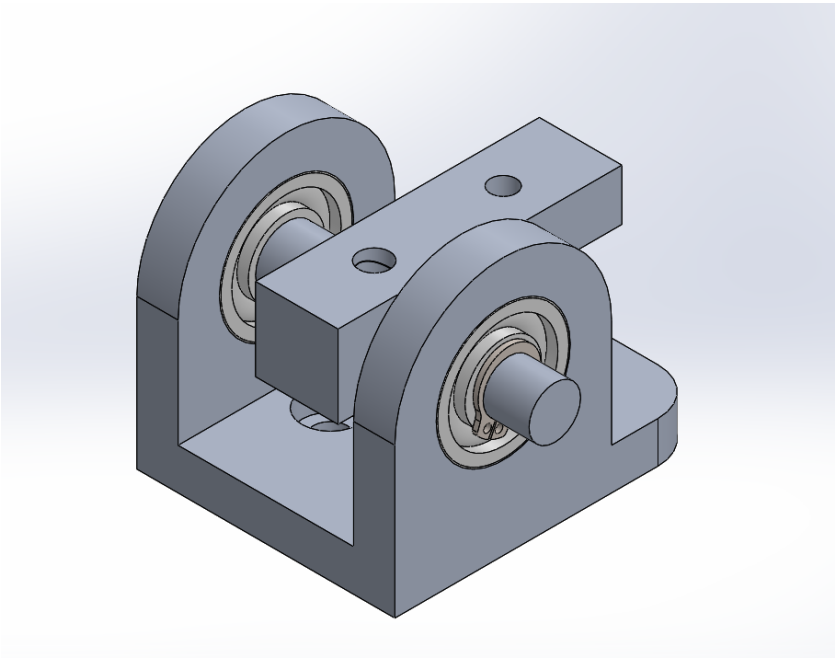

Figure C.2 Perspective of mechanism

Table C.1 Electronic equipments of measurement mechanism

Part	Description
Load cell	Futek LSB200 - #FSH00091
Amplifier	Futek IAA100 - #FSH03863

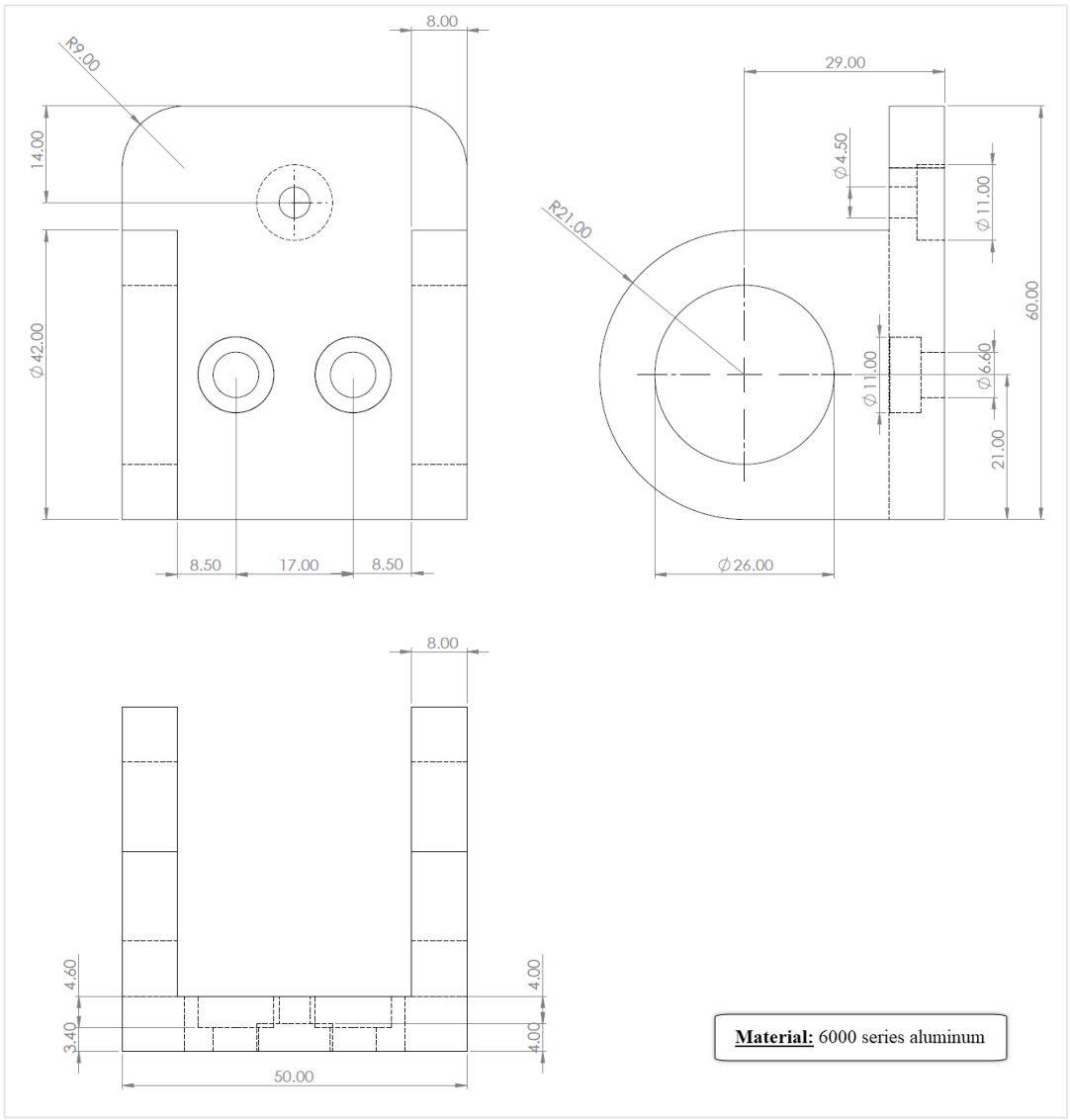

Figure C.3 Main body

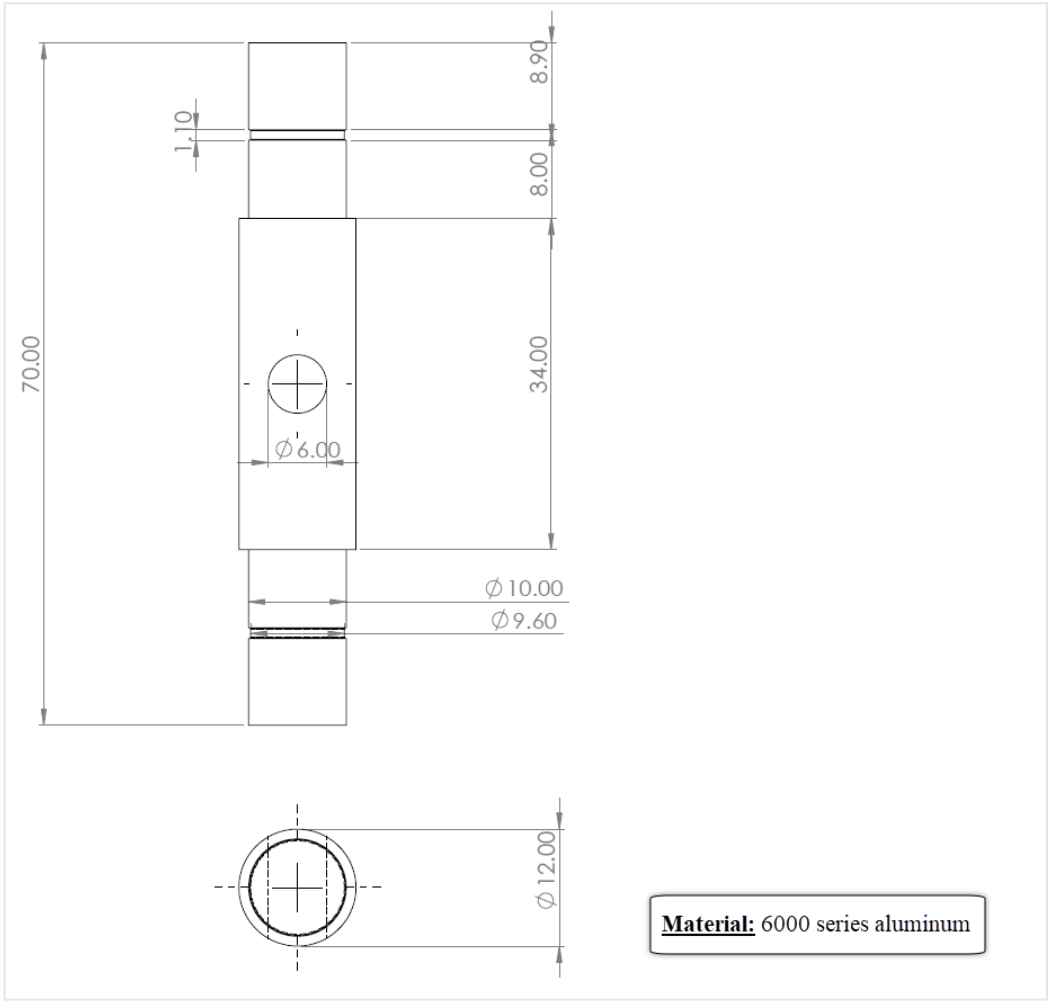

Figure C.4 Shaft

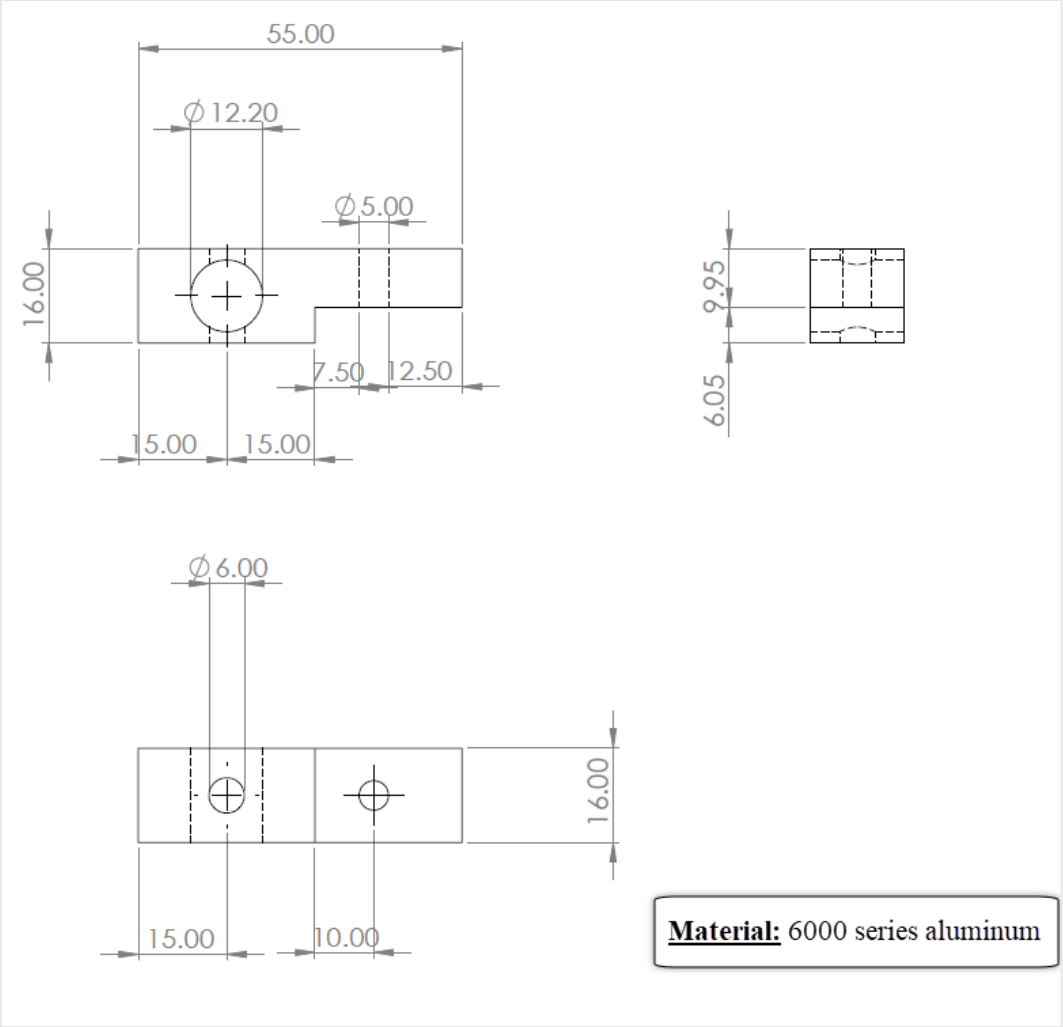

Figure C.5 Moment bar

APPENDIX D

CFD ANALYSIS

The solution volume was created with a 120-degree periodic model. Domain radius is 3.3 times the rotor outer radius. The same distance (3.3 times the rotor outer radius) is put upstream and downstream of the rotor. Therefore, the inlet to outlet domain extent is 6.6 times rotor outer radius.

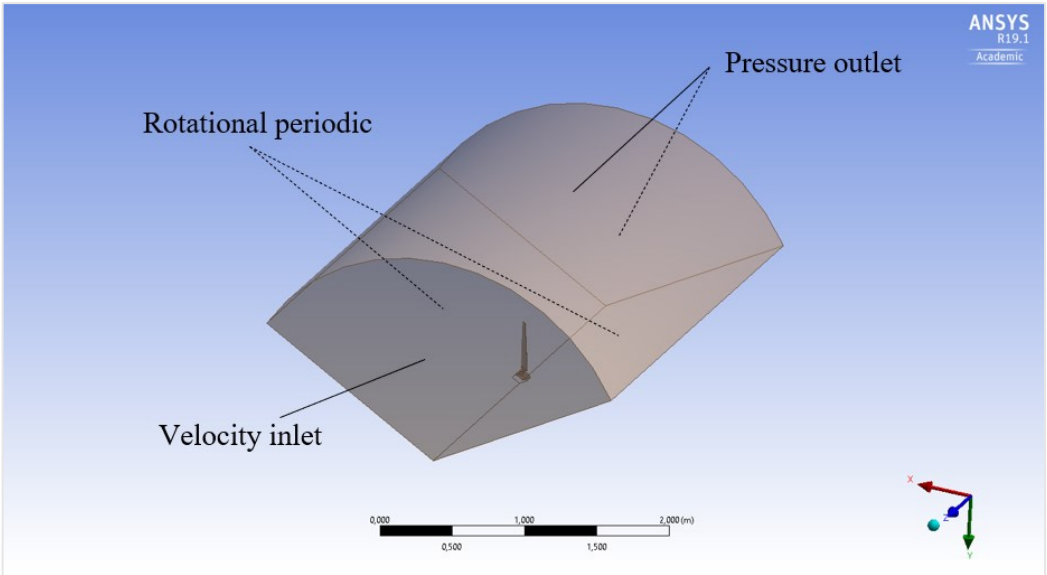

Figure D.1 Domain and boundary conditions

Inlet is velocity inlet and outlet is pressure outlet. As shown above, the domain outer radius is specified as Euler (inviscid) wall. Incompressible flow model is employed (density is 1.225 kg/s). Fluent settings are;

- Reynolds-averaged Navier Stokes (RANS) model
- Cell-Centered Finite Volume
- Coupled solver for pressure-velocity coupling
- Second order upwind scheme for convective terms
- Transition SST model for the turbulence (k-omega SST + gamma + ReynoldsTheta equations to model boundary layer transition from laminar to turbulent flow)

Table D.1 Studies of CFD analysis

	Study 1	**Study 2**	**Study 3**	**Study 4**
Number of mesh volume	2.8M	5.3M	14.1M	21M
Surface mesh size	1.2 mm	0.9 mm	0.6 mm	0.5 mm
Layers of boundary layer mesh	20	20	20	20
Far-field of mesh size	100 mm	100 mm	100 mm	50 mm
Mesh grow rate between blade and far-field volumes	1.20	1.15	1.10	1.10
y+	0.16	0.12	0.077	0.060
Power	0.32 W	0.32 W	0.37 W	0.39 W
Thrust force	0.33 N	0.32 N	0.32 N	0.32 N

CFD analysis was performed in four different mesh numbers and mesh independence was achieved for thrust force and power in the 4th study.

APPENDIX E

MODEL PLATFORM AND TURBINE ASSEMBLY

The dimensions of the spar type model platform designed by the members of IZTECH civil engineering hydromechanics laboratory are given in Figure E.1. Here, all dimensions are in centimeters.

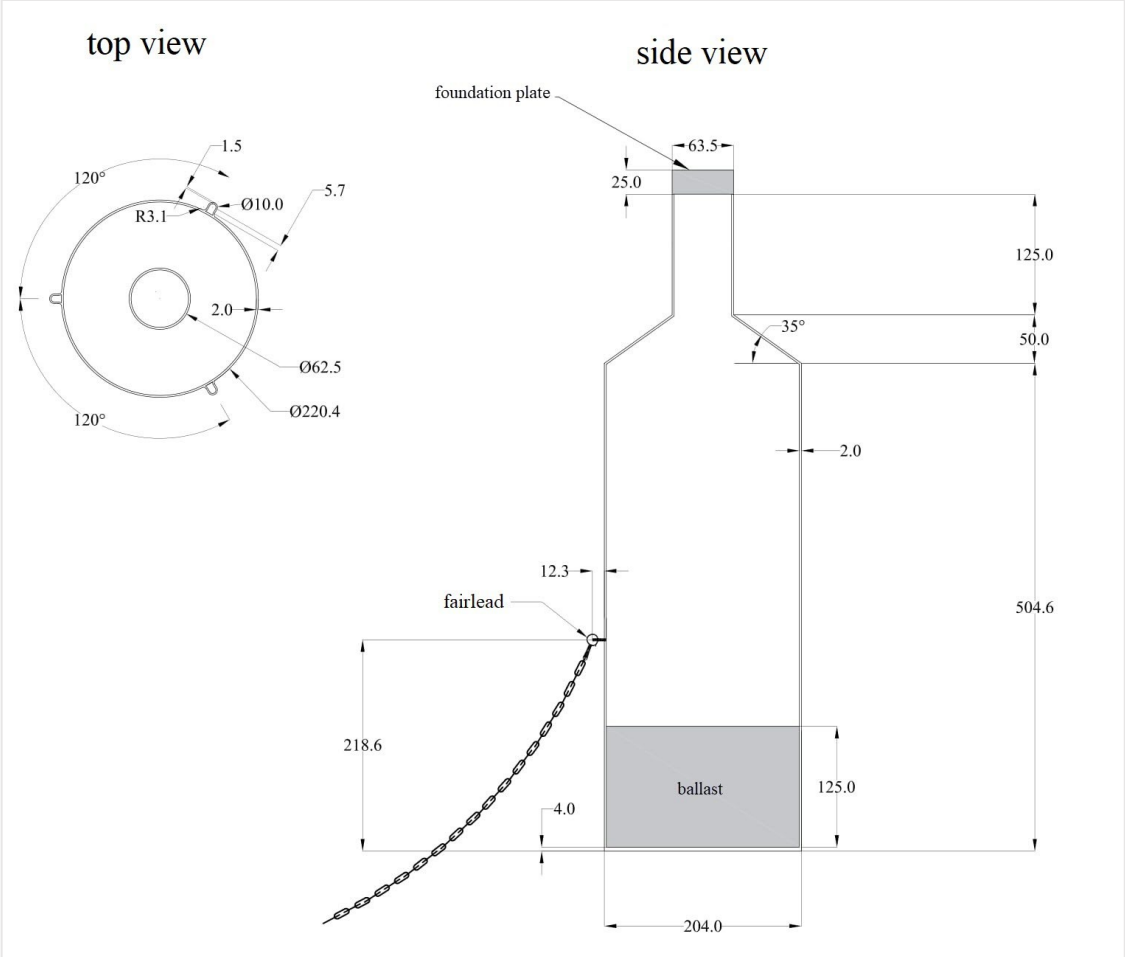

Figure E.1 Spar type model platform

The density values of the materials and materials used in the model platform are given in Table E.1.

Table E.1 Model platform malerials

Part	Material	Density
Main body and foundation plate	Stainless steel	7.90 ton/m^3
Ballast	Concrete	2.40 ton/m^3

Full assembly of the platform and turbine is given in Figure E.2. Center of gravity of model turbine, platform and assembly are shown.

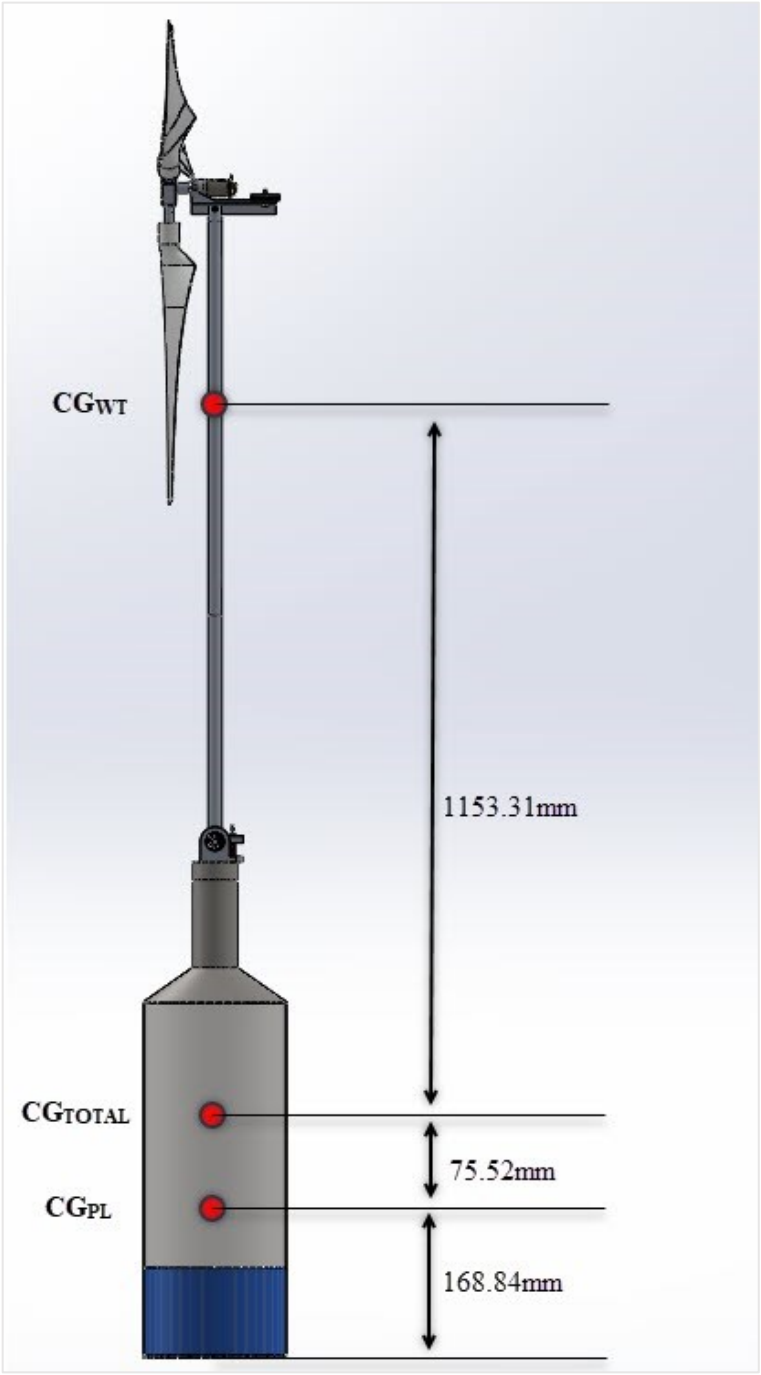

Figure E.2 Full assembly

REFERENCES

Anyoji, Masayuki, Taku Nonomura, Hikaru Aono, Akira Oyama, Kozo Fujii, Hiroki Nagai, and Keisuke Asai. 2014. "Computational and Experimental Analysis of a High-Performance Airfoil Under Low-Reynolds-Number Flow Condition." *Journal of Aircraft* 51:1864-1872. doi: 10.2514/1.C032553.

Azcona, José, Faisal Bouchotrouch, Marta González, Joseba Garciandía, Xabier Munduate, Felix Kelberlau, and Tor Nygaard. 2014. "Aerodynamic Thrust Modelling in Wave Tank Tests of Offshore Floating Wind Turbines Using a Ducted Fan." *Journal of Physics: Conference Series* 524:012089. doi: 10.1088/1742-6596/524/1/012089.

Bailey, Helen, Kate Brookes, and Paul Thompson. 2014. "Assessing Environmental Impacts of Offshore Wind Farms: Lessons Learned and Recommendations for the Future." *Aquatic biosystems* 10:8. doi: 10.1186/2046-9063-10-8.

Bayati, Ilmas, Marco Belloli, Luca Bernini, Hermes Giberti, and Alberto Zasso. 2017. "Scale model technology for floating offshore wind turbines." *IET Renewable Power Generation* 11. doi: 10.1049/iet-rpg.2016.0956.

Branlard, Emmanuel. 2017. *Wind Turbine Aerodynamics and Vorticity-Based Methods*. Vol. 7.

Brown, Douglas. 2009a. "Tracker video analysis and modeling tool." *Tracker, CA, accessed Dec* 27:2017.

Brown, Douglas. 2009b. "Video Modelling with Tracker." accessed 9 July. https://physlets.org/tracker/download/AAPT_video_modeling_2009.pdf.

Busby, Rebecca L. 2012. *Wind power. [electronic resource] : the industry grows up*: PennWell Corp. Bibliographies.

Cermelli, Christian, Dominique Roddier, and Alexia Aubault. 2009. *WindFloat: A Floating Foundation for Offshore Wind Turbines—Part II: Hydrodynamics Analysis*.

Chakrabarti, Subrata Kumar. 1994. *Offshore structure modeling*. Vol. 9: World Scientific.

Çengel, Yunus A., and John M. Cimbala. 2010. *Fluid mechanics : fundamentals and applications*. 2nd ed. ed, *Çengel series in engineering thermal-fluid sciences*: McGraw-Hill Higher Education. Non-fiction.

Drela, Mark. 1989. *XFOIL: An Analysis and Design System for Low Reynolds Number Airfoils*. Vol. 54.

Edinburg Design. 2016. "Wave Generators." accessed 5 July.

Guanche, Raul, Lucia Meneses, Javier Sarmiento, Cesar Vidal, and I. J. Losada. 2014. "Methodology to Obtain the Life Cycle Mooring Loads on a Semisubmersible Wind Platform." *Proceedings of the International Conference on Offshore Mechanics and Arctic Engineering - OMAE* 9. doi: 10.1115/OMAE2014-23668.

Gueydon, Sébastien, and Gerson Fernandes. 2013. "Scaling Methodology for Floating Wind Turbines." EWEA Offshore, Frankfurt, Germany.

Hepperle, Martin. 2018. "JavaFoil." accessed June 9, 2020. https://www.mh-aerotools.de/airfoils/javafoil.htm.

Hu, Yi, and Singiresu Rao. 2011. "Robust Design of Horizontal Axis Wind Turbines Using Taguchi Method." *Journal of Mechanical Design* 133:111009. doi: 10.1115/1.4004989.

International Renewable Energy Agency. 2020. "Wind Energy Data." accessed May 18, 2020. https://www.irena.org/wind.

Ishihara, Takeshi, Pham Phu, Hiroyuki Sukegawa, and Kenji Shimada. 2007. *A study on the dynamic response of a semi-submersible floating offshore wind turbine system Part 1: A water tank test*.

Kulunk, Emrah, and Nadir Yilmaz. 2009. *HAWT Rotor Design and Performance Analysis*.

Lange, Bernhard, Søren Larsen, Jørgen Højstrup, and R. Barthelmie. 2003. *The wind speed profile at offshore wind farm sites*.

Marten, David, and Juliane Peukert. 2013. *QBlade Guidelines v0.6*.

Marten, David, Juliane Peukert, Georgios Pechlivanoglou, Christian Nayeri, and Christian Paschereit. 2013. "QBLADE: An Open Source Tool for Design and Simulation of Horizontal and Vertical Axis Wind Turbines." *International Journal of Emerging Technology and Advanced Engineering* 3:264-269.

Martin, Heather. 2011. *Development of a Scale Model Wind Turbine for Testing of Offshore Floating Wind Turbine Systems*.

Olondriz Erdozain, Joannes, Josu Jugo, Iker Elorza, s Alonso-Quesada, and Aron Pujana-Arrese. 2019. "A Feedback Control Loop Optimisation Methodology for Floating Offshore Wind Turbines." *Energies* 12:3490. doi: 10.3390/en12183490.

Olsen, Frank, and Kim Dyre. 1993. "Vindeby Off-Shore Wind Farm - Construction and Operation." *Wind Engineering* 17 (3):120-128.

Owens, Brandon N. 2019. *The Wind Power Story: A Century of Innovation that Reshaped the Global Energy Landscape*: John Wiley & Sons.

Papadopoulos, Evangelos. 2007. "Heron of Alexandria (c. 10–85 AD)." In, 217-245.

Quinn, R., G. Schepers, and B. Bulder. 2016. "A Parametric Investigation Into the Effect of Low Induction Rotor (LIR) Wind Turbines on the Levelised Cost of Electricity for a 1 GW Offshore Wind Farm in a North Sea Wind Climate." *Energy Procedia* 94:164-172. doi: 10.1016/j.egypro.2016.09.213.

Rommel, D. P., D. Di Maio, and T. Tinga. 2020. "Calculating wind turbine component loads for improved life prediction." *Renewable Energy* 146:223-241. doi: https://doi.org/10.1016/j.renene.2019.06.131.

Schlichting, Hermann, and Klaus Gersten. 2016. *Boundary-layer theory*: Springer.

Schmidt, Wilhelm, and Heron von Alexandria. 1899. *Heron von Alexandria*: Teubner.

Shepherd, Dennis G. 1990. "Historical development of the windmill."

Shittu, Abdulhakim Adeoye, Ali Mehmanparast, Lin Wang, Konstantinos Salonitis, and Athanasios Kolios. 2020. "Comparative Study of Structural Reliability Assessment Methods for Offshore Wind Turbine Jacket Support Structures." *Applied Sciences* 10 (3). doi: 10.3390/app10030860.

Sutton, O. G. 1937. "The logarithmic law of wind structure near the ground." *Quarterly Journal of the Royal Meteorological Society* 63 (268):105-107. doi: 10.1002/qj.49706326820.

Tempel, J. 2006. "Design of Support Structures for Offshore Wind Turbines."

Tesla Institute. 2020. "Main components of wind turbine." accessed May 28, 2020. http://www.tesla-institute.com/index.php/renewable-energy-articles/213-main-components-of-a-wind-turbine.

Tran, Toan, and Dong-Hyun Kim. 2016. "A CFD study into the influence of unsteady aerodynamic interference on wind turbine surge motion." *Renewable Energy* 90:204-228. doi: 10.1016/j.renene.2015.12.013.

UIUC Applied Aerodynamics Group. 2020. "UIUC Airfoil Coordinates Databese." accessed June 17, 2020. https://m-selig.ae.illinois.edu/ads/coord_database.html.

Wulff, Hans Eberhard. 1966. *The traditional crafts of Persia*: MIT Press.

Zafar, Usman. 2018. *Literature Review of Wind Turbines*.